Reviews in Mineralogy & Geochemistry
Vol. 55, pp. 319-357, 2004

Fe Isotope Variations in the Modern and Ancient Earth and Other Planetary Bodies

Brian L. Beard and Clark M. Johnson

Department of Geology and Geophysics
University of Wisconsin-Madison
1215 West Dayton Street
Madison, Wisconsin 53706, U.S.A.

INTRODUCTION

Iron, the fourth most abundant element in the Earth's crust, has four naturally occurring stable isotopes: ^{54}Fe (5.84%), ^{56}Fe (91.76%), ^{57}Fe (2.12%), and ^{58}Fe (0.28%), and the natural, mass-dependent isotope variations of Fe in the rock record span a range of ~4 per mil (‰) in ^{56}Fe/^{54}Fe ratios (Fig. 1). The field of Fe isotope geochemistry is relatively new but has received considerable attention because it may allow us to gain a better understanding of how Fe is cycled in different environments. Iron typically occurs as either reduced ferrous Fe in oxygen-poor environments, or as oxidized ferric iron in oxygen-rich environments. Notably, only the reduced species is soluble in oxygenated aqueous solutions, unless the pH is low. In the Archean and Early Proterozoic, the earth may have been relatively oxygen-poor (e.g., Kasting et al. 1979; Grandstaff 1980; Holland 1994), suggesting that there may have been significant quantities of Fe (0.9 millimolar) dissolved in the oceans as $Fe(II)_{aq}$ (e.g., Ewers 1983; Sumner 1997). The extensive iron formations of Archean to Early Proterozoic age may have been deposited from such Fe(II)-rich oceans (e.g., Beukes and Klein 1992). In the modern oxic oceans, however, Fe contents are exceedingly low, <1 nanomolar in the open oceans (e.g., Martin and Gordon 1988; Bruland et al. 1991; Martin 1992; Johnson et al. 1997), and it is now recognized that marine productivity is Fe-limited in parts of the open oceans (e.g., Martin and Fitzwater 1988; Martin et al. 1989, 1994). The differences in the behavior of Fe with redox state, and the significant isotope fractionations (1‰ or more in ^{56}Fe/^{54}Fe) that are associated with redox conditions, suggests that Fe isotope studies will be extremely useful for tracing the Fe geochemical cycle.

The largest variations in Fe isotope compositions are associated with chemically precipitated sediments such as Pliocene to recent Fe-Mn crusts (Zhu et al. 2000) and Archean and Proterozoic age Banded Iron Formations (BIFs; Johnson et al. 2003a). Moreover, there is a similarly large range in the Fe isotope compositions of black shales, where diagenesis occurred under anoxic conditions (Yamaguchi et al. 2003; Matthews et al. 2004; Fig. 1). In contrast, clastic sedimentary materials such as loess, turbidites, the suspended load of rivers, and grey shales which were deposited in oxic environments have a very narrow range in Fe isotope compositions (Fig. 1; Beard et al. 2003a). The variability in Fe isotope compositions that is seen in nature, however, is not limited to low temperature sedimentary environments, where for example, chondritic meteorites, in particular individual chondrules, define a spread of ^{56}Fe/^{54}Fe ratios of 2.5‰ (e.g., Zhu et al. 2001; Kehm et al. 2003; Mullane et al. 2003a; Fig. 1). In contrast, bulk-rock analyses of achondrite meteorites (i.e., meteorites from differentiated planetary bodies) and terrestrial igneous rocks define a relative narrow range of Fe isotope

1529-6466/04/0055-010A$05.00

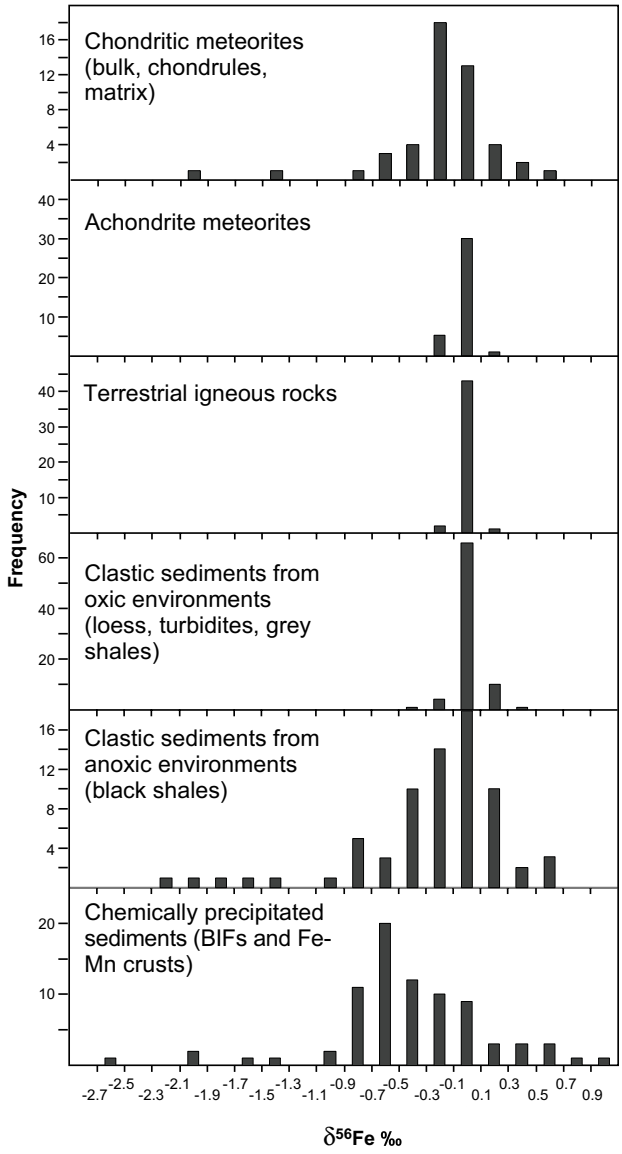

Figure 1. Frequency diagram of Fe isotope compositions measured in rocks from different environments. Interlaboratory bias in Fe isotope measurements have been corrected by normalizing to a δ^{56}Fe value of −0.09‰ for the IRMM-014 standard, which places Fe isotope measurements relative to the average of terrestrial igneous rocks. Data sources are: chondrite meteorite data from Zhu et al. (2001), Mullane et al. (2003a,b), and Kehm et al. (2003); achondrites including samples from the SNC, HED, Pallasite, and iron groups from Zhu et al. (2001), Mullane et al. (2003c), and Kehm et al. (2003); terrestrial igneous rocks from Beard et al. (2003b); clastic sediments from oxic environments including loess, turbidites, low-C_{org} shales, modern aerosols, and suspended river load sediments from Beard et al. (2003a); high-C_{org} black shales from Yamaguchi et al. (2003) and Matthews et al. (2004); chemically precipitated sediments including layers from Archean and Proterozoic Banded Iron Formations from Johnson et al. (2003a), and an Atlantic Ocean Fe-Mn crust from Zhu et al. (2000).

composition (Fig. 1). Indeed, terrestrial igneous rocks are very homogenous in Fe isotope compositions; the average of 43 igneous rocks that range in composition from peridotite to high-silica rhyolite are identical in $^{56}Fe/^{54}Fe$ ratios to within ±0.05‰ (1σ).

This chapter is divided into four main parts. In the first section, the nomenclature and analytical methods used in Fe isotope geochemistry are discussed. In the second section, we summarize the emerging data base of Fe isotope fractionation factors in abiological systems. The final two sections discuss Fe isotope variations in natural environments. In the third section, Fe isotope variability in high-temperature environments is reviewed and the variability of Fe isotope compositions in the solar system which may arise from planetary accretion processes and evaporation and condensation of Fe is highlighted. The final section discusses the variability of Fe isotope ratios measured on rocks and fluids from low-temperature environments. The origins of these Fe isotope variations may be evaluated based on Fe isotope fractionation factors, as well as mass-balance constraints that can be inferred from the growing database of Fe isotope compositions of natural samples. In the following chapter (Johnson et al. 2004), Fe isotope fractionations that are associated with biological processes are discussed and this provides a compliment to the review in the present chapter.

NOMENCLATURE AND ANALYTICAL METHODS

Nomenclature

Iron isotope data in the literature have been reported in both standard δ notation (parts per 10^3), and ε notation (parts per 10^4), and workers have reported data in terms of $^{57}Fe/^{54}Fe$, $^{57}Fe/^{56}Fe$, or $^{56}Fe/^{54}Fe$ ratios. The low abundance of ^{58}Fe limits its usefulness in describing mass-dependent variations, although ^{58}Fe may be important for evaluating non-mass dependent effects (e.g., Völkening and Papanastassiou 1989). In standard per mil notation, the $\delta^{56}Fe$ and $\delta^{57}Fe$ values are most commonly defined as:

$$\delta^{56}Fe = \left(\frac{^{56}Fe/^{54}Fe_{sample}}{\left(^{56}Fe/^{54}Fe_{standard}\right) - 1} \right) \times 10^3 \quad (1)$$

and

$$\delta^{57}Fe = \left(\frac{^{57}Fe/^{54}Fe_{sample}}{\left(^{57}Fe/^{54}Fe_{standard}\right) - 1} \right) \times 10^3 \quad (2)$$

Epsilon notation is defined similarly, although the deviations are in parts per 10,000. Comparison between these numbers is straightforward as shown in Figure 2, which plots the co-variations in $^{56}Fe/^{54}Fe$ and $^{57}Fe/^{54}Fe$ of layers from BIFs in both δ and ε notation. The mass-dependent fractionation line, based on a simple harmonic oscillator approximation (Criss 1999), lies close to a line of 1.5:1 for $\delta^{57}Fe$–$\delta^{56}Fe$ variations. For example, point A in Figure 2 has an $\delta^{57}Fe$ value of +15.0, which would be approximately equal to a $\delta^{56}Fe$ value of +1.00, as defined here, assuming normalization to an identical reference reservoir.

The choice of the reference reservoir for calculating δ or ε values is quite variable among different laboratories. Table 1 lists all the laboratories that have published Fe isotope data in an abstract or peer-reviewed journal as of September 2003, and include the form in which the data are reported (e.g., $\delta^{56}Fe$ or $\delta^{57}Fe$), as well as the reservoir or "standard" used to define δ or ε values. A common procedure of all labs currently conducting Fe isotope studies is to measure at least three Fe isotopes, which is done to provide a check on data quality, primarily evaluation of potential isobaric interferences. The choice of reference reservoir used in this chapter follows the approach of other stable isotope systems such as oxygen, which defines

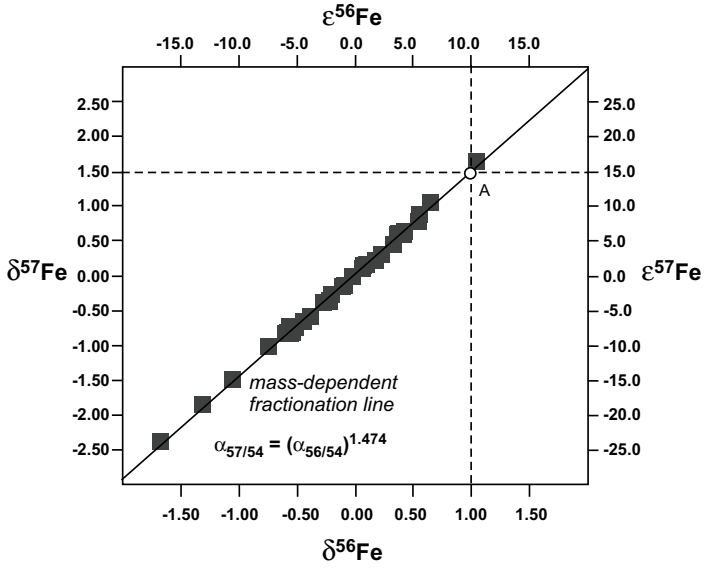

Figure 2. Co-variation of $^{56}Fe/^{54}Fe$ and $^{57}Fe/^{54}Fe$ ratios of individual layers from Banded Iron Formations, modified from Johnson et al. (2003a). The horizontal axis shows isotopic compositions in $\delta^{56}Fe$ (bottom) and $\varepsilon^{56}Fe$ (top), and the vertical axis shows values in $\delta^{57}Fe$ (left) and $\varepsilon^{57}Fe$ (right). Point A has a $\delta^{56}Fe$ of +1.00‰, which corresponds to an $\varepsilon^{57}Fe$ value of +15.0. Figure illustrates the multiple ways in which the same Fe isotope composition may be reported when isotopic variations are due to mass-dependent processes. See text for discussion.

Table 1. Laboratories pursuing Fe isotope studies and methods of reporting data.

Laboratory	Data Reporting	/ reservoir	Example Reference
CNRS Nancy	$\delta^{57}Fe$	IRMM-014	Rouxel et al. (2003)
DTM	$\delta^{56}Fe$	igneous rock	Kehm et al. (2003)
ETH	$\delta^{57}Fe$	IRMM-014	Poitrasson et al. (2002)
Frankfurt Min. Inst.	$\delta^{57}Fe$	IRMM-014	Weyer and Schwieters (2003)
Geol. Surv. Israel	$\delta^{57}Fe$	IRMM-014	Matthews et al. (2004)
London Royal Holloway	$\delta^{56}Fe$	IRMM-014	Archer and Vance (2002)
Luleå Univ. Tech.	$\delta^{56}Fe$	IRMM-014	Malinovsky et al. (2003)
MIT	$\delta^{56}Fe$	igneous rock	Bergquist and Boyle (2002)
Nat. Hist. Mus., London	$\delta^{56}Fe$	IRMM-014	Mullane et al. (2003a)
Oxford Univ.	$\varepsilon^{57}Fe$	IRMM-014	Zhu et al. (2000)
Rochester	$\delta^{56}Fe$	Canyon Diablo Troilite	Sharma et al. (2001)
UC Berkley	$\delta^{56}Fe$	igneous rock	Fantle and DePaolo (2002)
Univ. Bern	$\delta^{56}Fe$	IRMM-014	Walczyk and von Blackenburg (2002)
Univ. Southampton	$\delta^{56}Fe$	IRMM-014	Severmann et al. (2002)
Univ. WI-Madison	$\delta^{56}Fe$	avg. igneous rock	Beard and Johnson (1999)
USGS Menlo Park	$\delta^{56}Fe$	igneous rock BIR-1	Mandernack et al. (1999)

Note that many labs analyze at least three isotopes, and many data tables typically report both $^{56}Fe/^{54}Fe$ and $^{57}Fe/^{54}Fe$ isotope ratios. Conversion between igneous rock baselines and IRMM-014 baselines can be done using the IRMM-014 standard.

δ values relative to a significant planetary reservoir such as Standard Mean Ocean Water (SMOW). It is also an approach used in radiogenic isotopes where, for example, ε_{Nd}, ε_{Hf}, and γ_{Os} values are defined relative to a bulk earth or planetary reference value. Based on Table 1, the two main methods of reporting Fe isotope data are relative to terrestrial igneous rocks or relative to the IRMM-014 standard (available from the Institute of Reference Materials and Measurements, Belgium; Taylor et al. 1992, 1993). Regardless of the choice of reference reservoir, inter-laboratory comparison of Fe isotope ratios can be made by normalizing through a common standard such as IRMM-014, and this standard has rapidly become the accepted interlaboratory standard for the field. On an igneous rock scale, the $\delta^{56}Fe$ value of IRMM-014 is −0.09‰ and the $\delta^{57}Fe$ value is −0.11‰ (Beard et al. 2003b). All of the data discussed in this chapter are reported as $\delta^{56}Fe$ values relative to the average of igneous rocks (Beard et al. 2003b). Data from labs that only report $^{57}Fe/^{54}Fe$ values were converted by multiplying the $\delta^{57}Fe$ value by 0.667. For data reported relative to IRMM-014, −0.09‰ was subtracted from the $\delta^{56}Fe$ value to place it on the igneous rock scale.

Mass-dependent iron isotope fractionation between two phases, A and B, is noted as

$$\alpha_{A\text{-}B} = \frac{\left(^{56}Fe/^{54}Fe\right)_A}{\left(^{56}Fe/^{54}Fe\right)_B} \quad (3)$$

where, for example, an $\alpha_{A\text{-}B}$ of 1.001 means that phase A would have a $\delta^{56}Fe$ value 1‰ greater than phase B, based on the approximation that $10^3 ln\delta_{A\text{-}B}$ is ~ $\delta^{56}Fe_A$–$\delta^{56}Fe_B$.

Analytical methods

Iron isotope measurements are made by both the double-spike method using thermal ionization mass spectrometry (TIMS) (e.g., Johnson and Beard 1999; Beard and Johnson 1999; Beard et al. 1999; Mandernack et al. 1999; Bullen et al. 2001), as well as multi-collector inductively-coupled plasma mass spectrometry (MC-ICP-MS) (e.g., Belshaw et al. 2000; Sharma et al. 2001; Beard et al. 2003b; Kehm et al. 2003). The biggest benefit of TIMS-based double-spike analyses is that there are relatively few isobaric interferences associated with TIMS analyses (Albarède and Beard 2004), except for elemental isobars from ^{54}Cr on ^{54}Fe and ^{58}Ni on ^{58}Fe. The biggest difficulties using TIMS analysis are the lengthy amount of time required for each analysis (4-8 hours per analysis) and the low ionization efficiency of Fe, which limits TIMS Fe isotope analyses to working with microgram quantities of Fe. Most workers are pursuing Fe isotope studies by MC-ICP-MS because of the high ionization efficiency and rapid sample throughput. Instrumental mass bias corrections are made using bracketing standards (e.g., Belshaw et al. 2000; Beard et al. 2003b; Albarède and Beard 2004), or by comparison to mass bias inferred from an element spike, such as Cu or Ni, that has been added to the solution (e.g., Sharma et al. 2001; Kehm et al. 2003; Malinovsky et al. 2003; Albarède and Beard 2004).

Iron isotope analysis made using MC-ICP-MS presents special challenges because of isobars that are produced by the Ar plasma, including $^{40}Ar^{14}N$ on ^{54}Fe, $^{40}Ar^{16}O$ on ^{56}Fe, and $^{40}Ar^{16}OH$ on ^{57}Fe. Many workers have dealt with these isobars by using large quantities (~20 μg) of Fe during an isotopic analysis to minimize the relative intensities of Ar isobars, have employed cool-plasma techniques to eliminate Argides at the expense of decreased sensitivity, or used a narrow defining slit to allow Faraday collectors to be positioned to coincide with the Fe shoulder of a multi-species mass spectrum (e.g., Belshaw et al. 2000; Kehm et al. 2003; Weyer and Schwieters 2003). Other workers have utilized a collision cell to eliminate or greatly reduce Ar isobars, and this approach provides very high sensitivity, where high-precision Fe isotope analyses can be made on samples as small as 100 ng (Beard et al. 2003b). MC-ICP-MS analyses generally produce an external precision of 0.10 and 0.15‰ (2σ) for $^{56}Fe/^{54}Fe$ and $^{57}Fe/^{54}Fe$ ratios, respectively (e.g., Beard et al. 2003a;b).

The accuracy of Fe isotope compositions can be strongly affected by the purity of the sample. For example, there can be significant matrix effects that change instrumental mass bias for samples as compared to standards unless they are purified to similar degrees (Kehm et al. 2003; Albarède and Beard 2004). Indeed, in order to avoid these matrix affects the Fe concentrations of samples and standards must be carefully controlled (Kehm et al. 2003; Albarède and Beard 2004). Apparently the redox state of Fe in solution may be an issue as well (Zhu et al. 2002). Purification of the sample is important for minimizing matrix effects, as well as eliminating isobars from Cr and Ni, in addition to molecular isobars such as $^{40}Ca^{16}O$ on ^{56}Fe and $^{40}Ca^{16}OH$ on ^{57}Fe. It is important to stress, however, that during ion-exchange chromatography, yields must be quantitative in order to avoid laboratory-induced Fe isotope fractionations (e.g., Anbar et al. 2000; Roe et al. 2003). One of the best methods for demonstrating that the procedures used for purifying samples do not induce laboratory artifacts is to prepare artificial samples that match the chemical composition of the natural sample using Fe of known isotopic composition. Such a procedure was used by Beard et al. (2003a) to demonstrate the accuracy of Fe isotope compositions measured in Mid-Ocean Ridge (MOR) hydrothermal vent fluids.

ORIGIN OF Fe ISOTOPE VARIATIONS

Calculated fractionation factors

Calculation of stable isotope fractionation factors under equilibrium conditions provides important insight into expected isotopic fractionations, and the principles behind such calculations are discussed in detail in Schauble (2004). In the temperature range of 0–250°C, Fe isotope fractionations up to ~10‰ are predicted (Fig. 3), based on comparisons of reduced partition function ratios ($\delta_{56/54}$ factors; Schauble 2004). In general, calculated fractionation factors indicate that ferric Fe-bearing phases (aqueous or solid) will have higher $\delta^{56}Fe$ values than ferrous Fe-bearing phases (Fig. 3). The ferric Fe-bearing oxide minerals magnetite, hematite, goethite, and lepidocrocite, for example, are predicted to have higher $\delta^{56}Fe$ values than minerals that only contain ferrous Fe such as siderite, ankerite, and silicates such as olivine (Fig. 3A). In the case of aqueous Fe species, most ferric Fe-bearing species, such as $[Fe^{III}(H_2O)_6]^{3+}$, $[Fe^{III}(H_2O)_4Cl_2]^{+}$, and $[Fe^{III}Cl_4]^{-}$ are predicted to have higher $\delta^{56}Fe$ values than the hexaquo ferrous Fe complex $[Fe^{II}(H_2O)_6]^{2+}$ (Fig. 3B). Exceptions to the generalization that ferric Fe phases are expected to have the highest $\delta^{56}Fe$ values include pyrite, which is predicted to have the highest $\delta^{56}Fe$ values of the minerals illustrated in Figure 3A. In addition, in the case of the octahedral ferro- and ferri-cyanide complexes, the ferrous Fe-bearing species is predicted to have the higher $\delta^{56}Fe$ values (Fig. 3B). Finally, the octahedral ferric chloride complex is predicted to have some of the lowest $\delta^{56}Fe$ values (Fig. 3B). Of these exceptions, the only phase that is common in natural low-temperature environments is pyrite.

The calculated Fe isotope fractionation factors suggest that Fe isotope shifts will occur during several important geologic processes. At high temperatures, such as those commonly found in magmas (800–1000°C), only a few tenths per mil fractionation in $^{56}Fe/^{54}Fe$ ratios are predicted among the common silicate minerals, as well as between silicates and oxides such as ilmenite and spinel; slightly larger fractionations between silicates and magnetite are predicted at high temperatures (Polyakov and Mineev 2000). If we take, therefore, the $\beta_{56/54}$ factor for olivine as representative of silicate minerals in igneous and metamorphic rocks, the relatively high $\beta_{56/54}$ factors for weathering products such as ferric oxides or hydrous ferric Fe-bearing silicates such as celadonite suggest that chemical weathering should produce phases that have $\delta^{56}Fe$ values that are several ‰ greater than those of igneous or metamorphic protoliths (Fig. 3A). In contrast, Fe carbonates, which may form in relatively anoxic marine environments, are predicted to have $\delta^{56}Fe$ values that are 1–2‰ lower than those of igneous and metamorphic rocks (Fig. 3A).

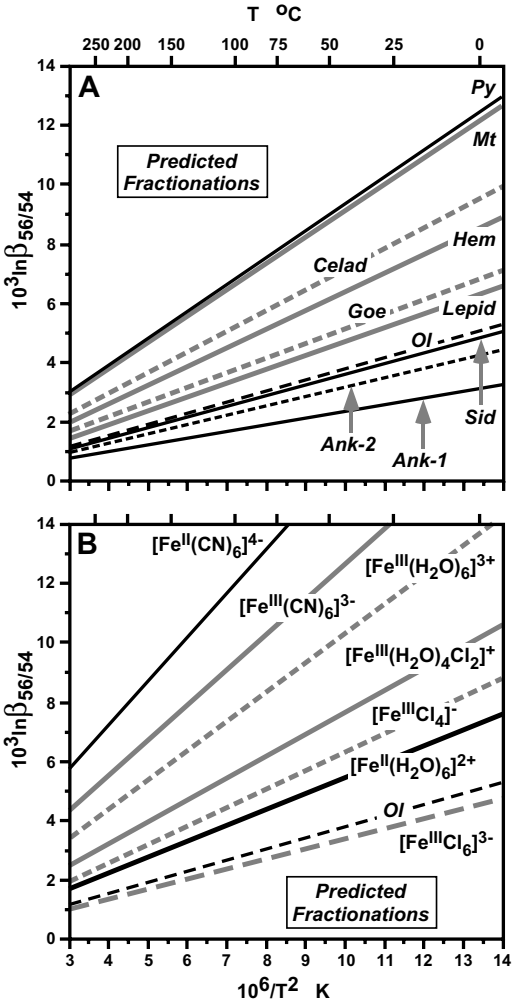

Figure 3. Plot of $10^3 \ln\beta_{56/54}$ values versus $10^6/T^2$ (K) for (A) Fe minerals calculated from Polyakov and Mineev (2000), and for (B) aqueous Fe species calculated from Schauble et al. (2001). Temperature scale in °C shown at top. Mineral abbreviations are Py: pyrite, Mt: magnetite, Celad: celadonite, Hem: hematite, Goe: goethite, Lepid: lepidocrocite, Ol: olivine, Sid: siderite, Ank-2: ankerite ($Ca_{1.1}Mg_{0.5}Fe_{0.3}Mn_{0.1}(CO_3)_2$), Ank-1: ankerite ($Ca_1Mg_{0.5}Fe_{0.5}(CO_3)_2$).

In the case of fluid-mineral fractionation involving Fe-bearing aqueous solutions, the $\beta_{56/54}$ factors for hexaquo ferric Fe are significantly higher than those of ferric Fe oxides (Fig. 3). In addition, the $\beta_{56/54}$ factors for hexaquo ferrous Fe are significantly higher than those of Fe carbonates (Fig. 3). These observations suggest that fluid-mineral Fe isotope fractionation factors for common natural fluids and minerals will tend to be positive, assuming no change in redox state for Fe. The predicted $\beta_{56/54}$ factors, however, suggest that significant changes in Fe isotope fractionations may occur depending on the structure of the mineral phase involved, even within a single group such as ferric oxides/hydroxides and Fe carbonates. For example, at low temperatures, the δ^{56}Fe values for hematite, goethite, and lepidocrocite are predicted to be different by several per mil, as are the Fe carbonates, including siderite and ankerite (Fig. 3A). In the case of aqueous Fe species, significant Fe isotope effects are predicted for Cl^- substitution into the hexaquo ferric Fe complex (Fig. 3B). Determination of the exact solid phase, as well as the aqueous Fe species involved, may therefore be important in interpreting Fe isotope fractionations that are expected in natural systems.

Experimental determination of fractionation factors

The large Fe isotope fractionations predicted to occur between aqueous ferric and ferrous Fe species (Fig. 3) has been investigated experimentally at two temperatures for hexaquo Fe(III) and Fe(II), as well as the effect of Cl^- substitution (Johnson et al. 2002; Welch et al. 2003). The kinetics of isotopic exchange in these experiments was determined using an enriched ^{57}Fe tracer for the ferric Fe phase. The ^{57}Fe tracer experiments reported in Johnson et al. (2002) and Welch et al. (2003) indicate that 95% isotopic equilibrium between $Fe(III)_{aq}$ and $Fe(II)_{aq}$ occurs within ~60 seconds at room temperature (22°C), or within ~5 minutes at 0°C. The relatively slower isotopic exchange rates at lower temperatures are expected.

Although isotopic equilibrium will be quickly attained between the hexaquo ferric Fe, hexaquo ferrous Fe, and monochloro ferric Fe complexes, the relatively rapid exchange rates presents a challenge in terms of separation of the two species for isotopic analysis. Johnson et al. (2002) and Welch et al. (2003) rapidly (~1 s) precipitated the ferric Fe fraction through carbonate addition, during which time approximately 10–20% isotopic exchange occurred between the aqueous ferric and ferrous Fe species, based on the isotope exchange kinetics determined from the enriched ^{57}Fe tracer experiments. The errors introduced by partial re-equilibration during species separation are largest for experiments using low $Fe(II)/Fe_T$ ratios, and this is the likely explanation for the deviations in $\delta^{56}Fe$ values for $Fe(II)_{aq}$ at low $Fe(II)/Fe_T$ ratios relative to that expected from isotopic mass balance (Fig. 4).

Welch et al. (2003) determined that $Fe(III)_{aq}$-$Fe(II)_{aq}$ fractionation at 22°C (corrected for partial re-equilibration) was +3.02 ± 0.14‰, +3.05 ± 0.17‰, and +2.92 ± 0.08‰ for solutions that contained 0, 11, and 111 mM Cl^-, respectively, which are all the same within error. At 0°C, the $Fe(III)_{aq}$–$Fe(II)_{aq}$ fractionation (corrected for partial re-equilibration) for the three Cl^- contents was +3.50 ± 0.31‰, +3.57 ± 0.17‰, and +3.65 ± 0.15‰. The consistent $Fe(III)_{aq}$-$Fe(II)_{aq}$ fractionations at a given temperature determined for a variety of solution compositions, and at different Fe(III) to total Fe ratios suggests that variations in the hydroxide and chloride species studied by Johnson et al. (2002) and Welch et al. (2003) has no significant isotopic effect. For example, the proportions of $[Fe^{III}(H_2O)_6]^{3+}$, $[Fe^{III}(H_2O)_5OH]^{2+}$, and $[Fe^{III}(H_2O)_5Cl]^{2+}$ in these solutions varied from 0.1 to 64%, 0.0 to 47%, and 0.0 to 44%, respectively, over the range of pH values and Cl^- contents studied by Johnson et al. (2002) and Welch et al. (2003), and yet the $Fe(III)_{aq}$-$Fe(II)_{aq}$ fractionations are the same within error when corrected for small extents of partial isotopic re-equilibration during species separation. This suggests that the equilibrium Fe isotope fractionation between $[Fe^{III}(H_2O)_6]^{3+}$ and at least its mononuclear hydroxy complex is negligible.

The insignificant effect of Cl^- substitution on the $Fe(III)_{aq}$–$Fe(II)_{aq}$ fractionation is somewhat surprising. Chloride substitution lowers the vibrational frequency of the Fe–Cl bond pair as compared to the Fe-O bond (248 versus 505 cm^{-1} for ν_3, and 184 versus 304 cm^{-1} for ν_4; see Schauble et al. 2001 and references within). If we assume that the difference in $\beta_{56/54}$ factors for $[Fe^{III}(H_2O)_6]^{3+}$ and $[Fe^{III}(H_2O)_5Cl]^{2+}$ is half that calculated for $[Fe^{III}(H_2O)_6]^{3+}$ and $[Fe^{III}(H_2O)_5Cl_2]^{+}$ by Schauble et al. (2001), we would expect a 1.5‰ difference in $\delta^{56}Fe$ values between $[Fe^{III}(H_2O)_6]^{3+}$ and $[Fe^{III}(H_2O)_5Cl]^{2+}$ at 22°C. Because the $[Fe^{III}(H_2O)_5Cl]^{2+}$ species ranged from 0 to 44% in the experiments of Welch et al. (2003), such a fractionation effect should have produced $Fe(III)_{aq}$-$Fe(II)_{aq}$ fractionations that varied by up to 0.7‰ and correlated with Cl^- contents, but this was not observed. Although the reason for the relative insensitivity of $Fe(III)_{aq}$-$Fe(II)_{aq}$ fractionations to Cl^- contents is not clear, this result greatly simplifies application of the measured Fe isotope fractionations to natural fluids, which may be quite variable in their chloride and hydroxide species. For example, seawater contains ~0.5 M Cl^-, 0.03 M SO_4^{2-}, and 0.002 M total CO_2, where dissolved ferrous speciation is dominated by $[Fe^{II}(H_2O)_6]^{2+}$ and ferric speciation is dominated by $[Fe^{III}(H_2O)_4(OH)_2]^{+}$ (>99%), $[Fe^{III}(H_2O)_5(OH)]^{2+}$, and $[Fe^{III}(OH)_3]^{0}$ (e.g., Millero et al. 1995); the results suggest

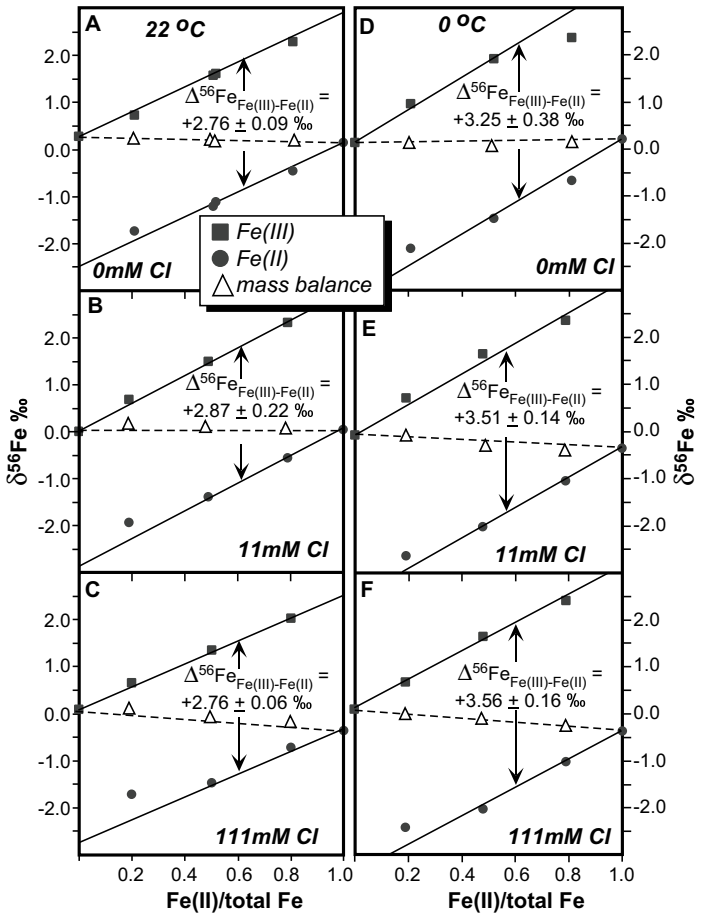

Figure 4. Isotopic mass-balance for measured δ^{56}Fe values of ferric (■) and ferrous (●) Fe in solution as a function of Fe(II)/Fe_T ratios. Although the initial Fe isotope compositions of the fluids have δ^{56}Fe values of ~0‰ (shown by dotted mixing line), the lighter Fe isotopes are portioned into the ferrous species following attainment of isotopic equilibrium. The triangles (△) represent the calculated isotopic mass balance of the different solutions. Fractionations noted are measured values based on data for equimolar and higher Fe(II)/total Fe ratio experiments. (A) and (D) are for experiments with zero Cl^- at 22 and 0°C, respectively. (B) and (E) are experiments done with at 11 mM Cl^- at 22 and 0°C, respectively. (C) and (F) are experiments done with 111 mM Cl^- at 22 and 0°C, respectively. Modified from Welch et al. (2003).

that these variations in speciation will have negligible isotopic effects relative to hexaquo Fe(III).

The experimentally measured temperature dependence of the $Fe(III)_{aq}$–$Fe(II)_{aq}$ fractionation at low temperatures is:

$$10^3 \ln\alpha_{Fe(III)_{aq}\text{-}Fe(II)_{aq}} = A \times \frac{10^6}{T^2} + B \qquad (4)$$

where A = 0.334 ± 0.032 and B= −0.88 ± 0.38, based on the determinations at 0 and 22°C by

Welch et al. (2003). This produces a temperature dependence that is similar to that calculated by Schauble et al. (2001), but is displaced to $Fe(III)_{aq}$–$Fe(II)_{aq}$ fractionations that are approximately half that predicted by Schauble et al. (2001). This discrepancy lies outside the estimated uncertainties for the predicted and measured $Fe(III)_{aq}$–$Fe(II)_{aq}$ fractionations (Fig. 5). Based on comparison of measured $Fe(III)_{aq}$-hematite fractionations with those predicted from spectroscopic data, Skulan et al. (2002) noted that the predicted $Fe(III)_{aq}$–hematite and $Fe(III)_{aq}$–$Fe(II)_{aq}$ fractionations may be brought into closer agreement with the measured $Fe(III)_{aq}$–hematite and $Fe(III)_{aq}$–$Fe(II)_{aq}$ fractionations if the $\beta_{56/54}$ factor for $[Fe^{III}(H_2O)_6]^{3+}$ from Schauble et al. (2001) is reduced by 1–2‰ at low temperatures, and this suggestion has been supported by recent ab inito calculations of the $\beta_{56/54}$ factor for $[Fe^{III}(H_2O)_6]^{3+}$ by Anbar et al. (2004; Fig. 5).

There does appear to be small (~0.1‰) Fe isotope fractionations between some Fe(III) chloro-complexes at very high Cl concentrations (e.g., 7–2 M HCl; Anbar et al. 2000; Roe et al. 2003). Based on a series of anion-exchange resin experiments using aqueous Fe(III) solutions in 7 and 2 M HCl, Anbar et al. (2000) and Roe et al. (2003) inferred that there is a small (~0.1‰) fractionation between Fe(III) that is tetrahedrally complexed with Cl^- relative to Fe(III) that is octahedrally coordinated with water and chloride ions. Matthews et al. (2001) showed that aqueous Fe species that are complexed by organic ligands may record significant Fe isotope fractionation where $Fe(II)_{aq}$ and $Fe(III)_{aq}$ that was bound with 2, 2′- bipyridine and chloride ions, respectively, recorded fractionations up to 12‰. The isotopic fractionations were interpreted to reflect kinetic effects due to the relatively slow separation process, as well as breakdown of $[Fe^{II}(bipy)_3]^{2+}$ in the 6M HCl solution. Although, as noted by Matthews et al. (2001), the measured isotopic fractionations do not reflect equilibrium isotope partitioning, they do highlight the importance of highly covalent bonds, where, in this case, ferrous Fe is enriched in $^{56}Fe/^{54}Fe$ ratios relative to ferric Fe chloro complexes.

Skulan et al. (2002) investigated Fe isotope fractionation between aqueous Fe(III) and hematite at 98°C. During the initial stages of this reaction (12 hours), at a rapid hematite

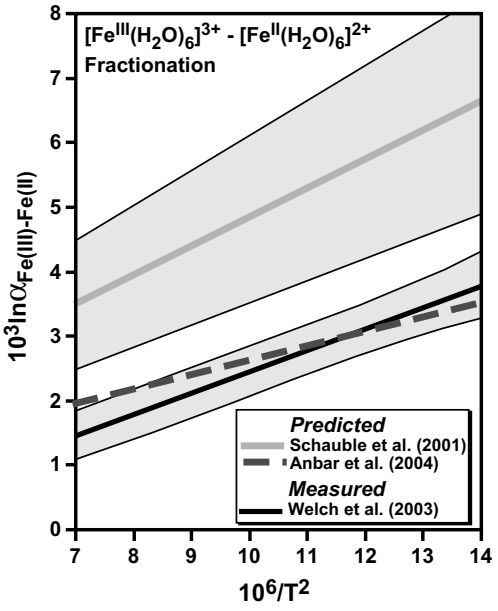

Figure 5. Plot of $10^3 \ln\alpha_{Fe(III)aq\text{-}Fe(II)aq}$ versus $10^6/T^2$ (K) for the calculated fractionation factor between $[Fe^{III}(H_2O)_6]^{3+}$–$[Fe^{II}(H_2O)_6]^{2+}$ by Schauble et al. (2001) and Anbar et al. (2004), as compared to the experimentally-determined curve of Welch et al. (2003). The grey shaded fields are 2σ errors (field omitted for study of Anbar et al. (2004) for simplicity).

precipitation rate, the Fe isotope fractionation between hematite and Fe(III) can be modeled as a Rayleigh distillation process using $\Delta_{Fe(III)\text{-hematite}} = +1.3‰$ (Skulan et al. 2002). This rapidly synthesized hematite is isotopically zoned as determined by step-wise leaching of hematite after 98% precipitation. Skulan et al. (2002) inferred that initial rapid hematite synthesis resulted in kinetic Fe isotope fractionations because in longer-term experiments the measured Fe isotope fractionation factor between Fe(III) and hematite is a strong function of time (Fig. 6). Based on a series of long-term experiments (up to 203 days) that involved a variety of hematite synthesis rates and initial conditions, Skulan et al. (2002) extrapolated the Fe(III)-hematite fractionation to a zero precipitation rate (Fig. 7), and inferred this to be the best estimate of the equilibrium fractionation factor. Additionally, Skulan et al. (2002) applied a small correction (~0.2‰) to these data to subtract the effects of the large initial kinetic isotope fractionation (Fig. 6) that were not completely erased during the long-term experiments. This correction, which Skulan et al. (2002) define as the "terminal offset" is a small correction that is based on modeling of the extent of dissolution and re-precipitation based on parallel experiments that used enriched ^{57}Fe tracers. Extrapolation of the data corrected for the "terminal offset" to a zero hematite precipitation rate yields a $\Delta_{Fe(III)\text{-hematite}}$ fractionation of $-0.10 \pm 0.20‰$ at 98°C (Fig. 7).

Composite effects of equilibrium and kinetic fractionations in an experiment

The preceding discussion suggests that, in general, isotopic equilibrium is attained between aqueous Fe species within minutes, whereas kinetic isotope fractionation is likely to be significant during rapid precipitation of minerals from fluids, particularly where precipitation occurs over timescales of hours or even days. Oxidation of aqueous Fe(II), followed by precipitation of ferric oxide/hydroxides, is a common process in near-surface environments, where $Fe(II)_{aq}$ may be supplied by hydrothermal sources or anoxic groundwaters (Bullen et al. 2001), and consideration of combined equilibrium and kinetic effects during such processes is important to understanding the Fe isotope variations that may be produced. If we assume that precipitation of ferric Fe minerals from $Fe(II)_{aq}$ is preceded by formation of aqueous Fe(III), the overall process may be envisioned to occur in two steps:

$$Fe(II)_{aq} \rightarrow Fe(III)_{aq} \rightarrow Fe(OH)_3(s) \quad (5)$$

where the ferric Fe hydroxide precipitate, most likely ferrihydrite, is represented as $Fe(OH)_3$

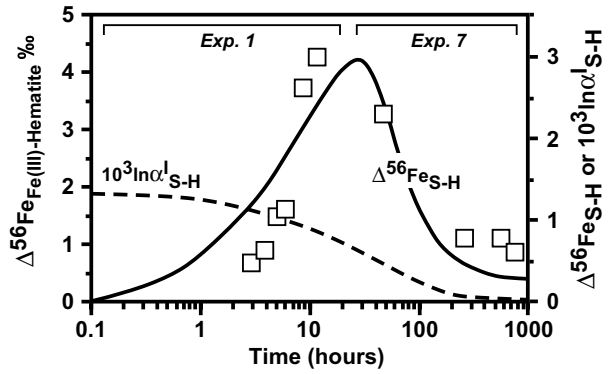

Figure 6. Superposition of a model for the $\Delta^{56}Fe_{Fe(III)\text{-hematite}}$ (solid line) and the assumed instantaneous $10^3 \ln\alpha^I_{Fe(III)\text{-hematite}}$ fractionation (dashed line) with time relative to measured experimental data (□) from the study of $Fe(III)_{aq}$-hematite fractionation by Skulan et al. (2002). Over short timescales (≤12 h), kinetic isotope fractionation dominates, whereas over longer timescales, the isotopic fractionations move back toward a near-zero value. Scale for measured data on left and bottom, whereas scale for model curves is on right. Adapted from Skulan et al. (2002).

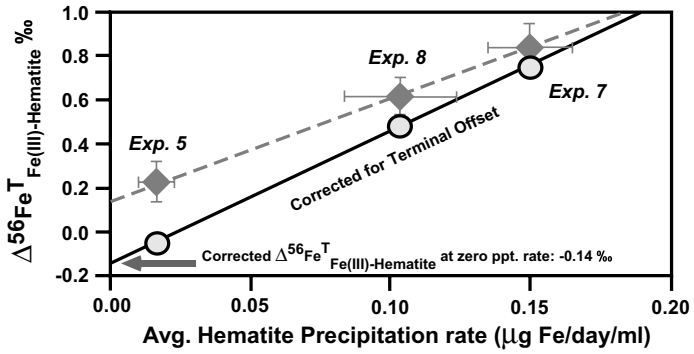

Figure 7. Measured and corrected $\Delta^{56}Fe^{T}_{Fe(III)\text{-}Hematite}$ values (◆ and ○, respectively) relative to average hematite precipitation rate for Experiments 5, 7, and 8 of Skulan et al. (2002). The $\Delta^{56}Fe^{T}_{Fe(III)\text{-}Hematite}$ values are defined as those measured at the termination of the experiments; the corrected $\Delta^{56}Fe^{T}_{Fe(III)\text{-}Hematite}$ values reflect the estimated correction required to remove any residual kinetic isotope fractionation that was produced early in experiments that was not completely removed by dissolution and re-precipitation over the long term. Extrapolation of the corrected $\Delta^{56}Fe^{T}_{Fe(III)\text{-}Hematite}$ values to zero precipitation rates yields an estimate for the equilibrium $Fe(III)_{aq}$–hematite fractionation, $\Delta^{56}Fe_{Fe(III)\text{-}hematite}$, of −0.14‰. Modified from Skulan et al. (2002).

for simplicity. Bullen et al. (2001) measured the overall Fe isotope fractionation produced by oxidation of $Fe(II)_{aq}$, followed by precipitation to ferrihydrite, and the overall reaction in their batch experiment is well fit by a first-order rate law (Fig. 8). It is important to note, however, that Bullen et al. (2001) interpret their data in a different conceptual framework than that of Equation (5), instead focusing on Fe isotope exchange between aqueous ferrous Fe hydroxide species. The motivation for re-evaluating this framework lies in the subsequent studies of Fe isotope exchange between $Fe(II)_{aq}$ and $Fe(III)_{aq}$ by Johnson et al. (2002) and Welch et al. (2003), both in terms of rates of exchange and magnitude of fractionation. Assuming that Equation (5) is applicable to oxidation of $Fe(II)_{aq}$ to $Fe(III)_{aq}$, followed by precipitation of ferric Fe hydroxide, we may define a series of first-order rate equations to describe the overall process:

$$\frac{d\left[\mathrm{Fe(II)_{aq}}\right]}{dt} = -k_1\left[\mathrm{Fe(II)_{aq}}\right] \tag{6}$$

$$\frac{d\left[\mathrm{Fe(III)_{aq}}\right]}{dt} = k_1\left[\mathrm{Fe(II)_{aq}}\right] - k_2\left[\mathrm{Fe(III)_{aq}}\right] \tag{7}$$

$$\frac{d\left[\mathrm{Fe(OH)_3}\right]}{dt} = k_2\left[\mathrm{Fe(III)_{aq}}\right] \tag{8}$$

where k_1, and k_2 are first-order rate constants. The size of the $Fe(III)_{aq}$ component will therefore be determined by the k_2/k_1 ratio, where increasing k_2/k_1 ratios will produce a decreasing proportion of $Fe(III)_{aq}$.

Equations (6)–(8) predict that the proportions of $Fe(II)_{aq}$, $Fe(III)_{aq}$, and $Fe(OH)_3(s)$ will change over time. However, if the rate of Fe isotope exchange is rapid between, for example, $Fe(II)_{aq}$ and $Fe(III)_{aq}$, Fe isotope equilibrium may still be maintained between aqueous Fe species, and this may be evaluated through comparison of the residence time of $Fe(III)_{aq}$ relative to the time required to attain isotopic equilibrium between $Fe(II)_{aq}$ and $Fe(III)_{aq}$. The residence time (τ) of $Fe(III)_{aq}$ may be defined as:

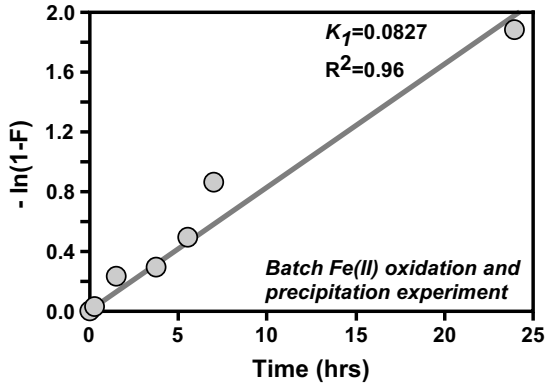

Figure 8. Regression of batch oxidation and precipitation experiment of Bullen et al. (2001), where $Fe(II)_{aq}$ was oxidized, followed by precipitation of ferrihydrite, over a 24 h period. The reaction progress (F) is well-fit by a first-order rate law, where the rate constant is 0.0827 F/h, with an R^2 of 0.96. In the model illustrated by Equations (5)–(8) in the text, this rate constant would be set to k_1.

$$\tau_{Fe(III)_{aq}} = \frac{M_{Fe(III)_{aq}}}{J_{Fe(III)_{aq}}} \tag{9}$$

where $M_{Fe(III)aq}$ is the total moles of Fe in the $Fe(III)_{aq}$ reservoir, and $J_{Fe(III)aq}$ is the flux of Fe through the $Fe(III)_{aq}$ reservoir. Substituting the rate equations into Equation (9), we obtain:

$$\tau_{Fe(III)_{aq}} = \frac{\left[Fe(III)_{aq}\right]}{k_1\left[Fe(OH)_3\right] - k_2\left[Fe(III)_{aq}\right]} \tag{10}$$

If the time to reach isotopic equilibrium through isotopic exchange is t_{ex}, isotopic equilibrium between $[Fe(II)_{aq}]$ and $[Fe(III)_{aq}]$ should be maintained when:

$$\tau_{Fe(III)_{aq}} \gg t_{ex} \tag{11}$$

Based on the ^{57}Fe tracer work of Johnson et al. (2002) and Welch et al. (2003), the time required to attain isotopic equilibrium between $Fe(III)_{aq}$ and $Fe(II)_{aq}$ is on the order of a few minutes or less in dilute aqueous solutions.

In Figure 9, the proportions of $Fe(II)_{aq}$, $Fe(III)_{aq}$, and $Fe(OH)_3(s)$ over time are illustrated, as well as the residence time of $Fe(III)_{aq}$, as calculated using Equations (6)–(11), and the rate for k_1 from Figure 8. The time required to reach steady-state conditions in terms of the $Fe(III)_{aq}$/$Fe(II)_{aq}$ ratio is, of course, dependent upon the k_2/k_1 ratio, and varies from ~2 hours for k_2/k_1 = 50, to ~20 hours for k_2/k_1 = 5 (Fig. 9). It is important to note, however, that attainment of isotopic equilibrium between $Fe(II)_{aq}$ and $Fe(III)_{aq}$ is not related to the time required to reach steady-state in terms of the concentration or molar ratios of Fe in various species, because t_{ex} is entirely independent of the rate equations and rate constants of Equations 6-8. For the range of k_2/k_1 ratios illustrated in Figure 9, the residence time for $Fe(III)_{aq}$ greatly exceeds that of the time required for isotopic exchange after one hour or less into the experiment (Fig. 9), indicating that isotopic equilibrium between $Fe(II)_{aq}$ and $Fe(III)_{aq}$ should have been maintained for essentially the entire duration of the batch precipitation experiment of Bullen et al. (2001).

The calculations illustrated in Figure 9 demonstrate that attainment of steady-state conditions in terms of elemental abundances may not be related to attainment of isotopic equilibrium. The converse may also be true, a system that is at equilibrium in terms of concentrations may be far from isotopic equilibrium. Moreover, a system at steady-state conditions in terms of concentrations may also be far from isotopic equilibrium. This case is well illustrated by the experiments on $Fe(III)_{aq}$-hematite fractionations discussed above (Skulan et al. 2002). In Skulan et al.'s (2002) experiments, approximately constant $Fe(III)_{aq}$ contents

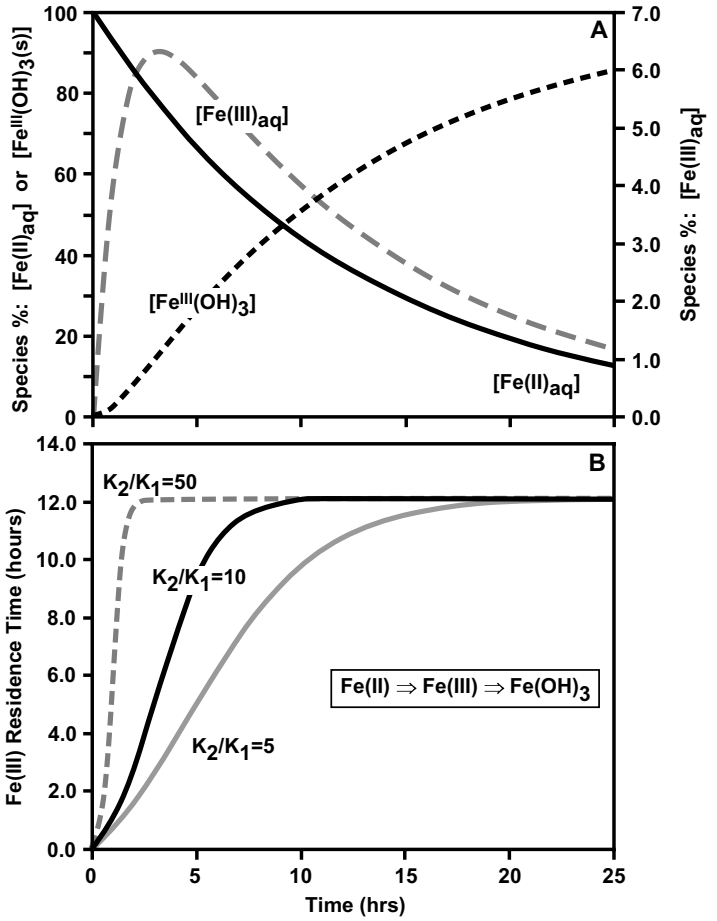

Figure 9. Proportions of species over time for the process of oxidation of $Fe(II)_{aq}$ to $Fe(III)_{aq}$, followed by precipitation of ferrihydrite (Eqn. 5), as calculated using the first-order rate laws of Equations (6)–(8), and the rate constant k_1 from Figure 8. (A) Proportion of species calculated from Equations (6)–(8), assuming a k_2/k_1 ratio of 10. Ferrihydrite represented as $Fe(OH)_3$ for simplicity. (B) The residence time of intermediate species $Fe(III)_{aq}$, as calculated using Equation (10), for various k_2/k_1 ratios.

were maintained through dissolution and reprecipitation processes—which were in approximate balance—but where large changes in $Fe(III)_{aq}$-hematite fractionations were measured over time as early Fe isotope fractionations produced by rapid hematite precipitation were progressively erased by slow dissolution and reprecipitation (Fig. 6). We note that our analysis of the process of oxidation and precipitation is different than that of Anbar (2004), where we explicitly consider the residence time of Fe relative to the time required for isotopic exchange.

We now turn to the Fe isotope fractionations that are predicted by a model where oxidation of $Fe(II)_{aq}$ to $Fe(III)_{aq}$ occurs, followed by precipitation of $Fe(III)_{aq}$ to ferrihydrite (FH) (Eqn. 5). In a closed system, the $\delta^{56}Fe$ values of the three components are constrained by simple mass balance as:

$$\delta_{SYS} = X_{Fe(II)aq}\delta_{Fe(II)aq} + X_{Fe(III)aq}\delta_{Fe(III)aq} + X_{FH}\delta_{FH} \quad (12)$$

where X represents the mole fractions of the three components (Eqn. 5).

In the case of the aqueous Fe components, the isotopic mass-balance relation is:

$$\delta_{(Fe_{aq})_T} = \frac{X_{Fe(II)_{aq}}}{X_{Fe(II)_{aq}} + X_{Fe(III)_{aq}}} \delta_{Fe(II)_{aq}} + \frac{X_{Fe(III)_{aq}}}{X_{Fe(II)_{aq}} + X_{Fe(III)_{aq}}} \delta_{Fe(III)_{aq}} \quad (13)$$

If the fractionation factor between $Fe(III)_{aq}$ and $Fe(II)_{aq}$ is:

$$\Delta_{Fe(III)_{aq}-Fe(II)_{aq}} = \delta_{Fe(III)_{aq}} - \delta_{Fe(II)_{aq}} \quad (14)$$

then Equation (13) can be simplified as:

$$\delta_{(Fe_{aq})_T} = \delta_{Fe(III)_{aq}} - \left(\Delta_{Fe(III)_{aq}-Fe(II)_{aq}}\right)\left(\frac{X_{Fe(II)_{aq}}}{X_{Fe(II)_{aq}} + X_{Fe(III)_{aq}}}\right) \quad (15)$$

where $\delta_{(Fe_{aq})_T}$ is the $\delta^{56}Fe$ value of the total aqueous Fe pool ($Fe(II)_{aq}$ and $Fe(III)_{aq}$), and $X_{Fe(II)}$ and $X_{Fe(III)}$ are the mole fractions of $Fe(II)_{aq}$ and $Fe(III)_{aq}$ in the total system, respectively. As precipitation of $Fe(III)_{aq}$ to ferrihydrite proceeds, the ratio of $\{X_{Fe(II)aq}/(X_{Fe(II)aq} + X_{Fe(III)aq})\}$ increases, and becomes unity when precipitation of $Fe(III)_{aq}$ is complete. Accordingly, if the value of $\Delta_{Fe(III)\text{-}Fe(II)}$ is constant (i.e., isotopic equilibrium is maintained), large changes will occur in the $\delta^{56}Fe$ value of the remaining aqueous Fe components. If the proportion of $Fe(III)_{aq}$ is small, as would be the case for high k_2/k_1 ratios (Fig. 9), the $\{X_{Fe(II)aq}/(X_{Fe(II)aq} + X_{Fe(III)aq})\}$ ratio is close to unity, and $\delta_{(Fe_{aq})_T}$ is equal to $\delta_{Fe(II)aq}$. In this case Equation (15) may be re-arranged to be equal to

$$\delta_{Fe(II)aq} - \delta_{FH} \approx \Delta_{Fe(III)\text{-}FH} - \Delta_{Fe(III)\text{-}Fe(II)} \quad (16)$$

where we define the fractionation factor between $Fe(III)_{aq}$ and ferrihydrite (FH) as:

$$\Delta_{Fe(III)aq\text{ - }FH} = \delta_{Fe(III)aq} - \delta_{FH} \quad (17)$$

Equation (16) notes that the difference in measured $\delta^{56}Fe$ values for $Fe(II)_{aq}$ and ferrihydrite precipitate is equal to difference in the $Fe(III)_{aq}$–ferrihydrite and $Fe(III)_{aq}$–$Fe(II)_{aq}$ fractionation factors, assuming that the proportion of $Fe(III)_{aq}$ is very small (≤5%). In cases where the proportion of $Fe(III)_{aq}$ ratio is significant (>5%), the isotopic effects of combined oxidation and precipitation may still be calculated using an incremental approach and Equation (12), along with the pertinent fractionations between components (Eqns. 14 and 17).

The usefulness of Equation (16) lies in its ability to show that the measured fractionation between $Fe(II)_{aq}$ and ferrihydrite precipitate of the experiments of Bullen et al. (2001), under conditions of high $Fe(II)_{aq}/Fe(III)_{aq}$ ratio and maintenance of isotopic equilibrium between $Fe(III)_{aq}$ and $Fe(II)_{aq}$, likely reflects the combined effects of an equilibrium $Fe(III)_{aq}$-$Fe(II)_{aq}$ fractionation and a fractionation between $Fe(III)_{aq}$ and ferrihydrite. For example, the −0.9‰ fractionation between aqueous Fe (which existed as essentially all ferrous Fe; T. Bullen, pers. commun. 2002) and ferrihydrite precipitate early in the experiment probably reflects the combined effects of two fractionation steps: a +2.9‰ equilibrium fractionation between $Fe(III)_{aq}$ and $Fe(II)_{aq}$, and a +2.0‰ fractionation between $Fe(III)_{aq}$ and ferrihydrite upon precipitation (e.g., Eqn. 16).

The combined effects of a +2.9‰ equilibrium fractionation between $Fe(III)_{aq}$ and $Fe(II)_{aq}$, and a +2.0‰ fractionation between $Fe(III)_{aq}$ and ferrihydrite upon precipitation is illustrated in Figure 10. Although a k_2/k_1 ratio of 5 appears to fit the fractionations measured by Bullen et al. (2001) (Fig. 10), we note that at these relatively low k_2/k_1 ratios, Equation (16) cannot be used, but instead the calculations are made using an incremental approach and simple isotope mass-balance equations (e.g., Eqn. 12). As the k_2/k_1 ratio increases to ~20, Equation (16) may

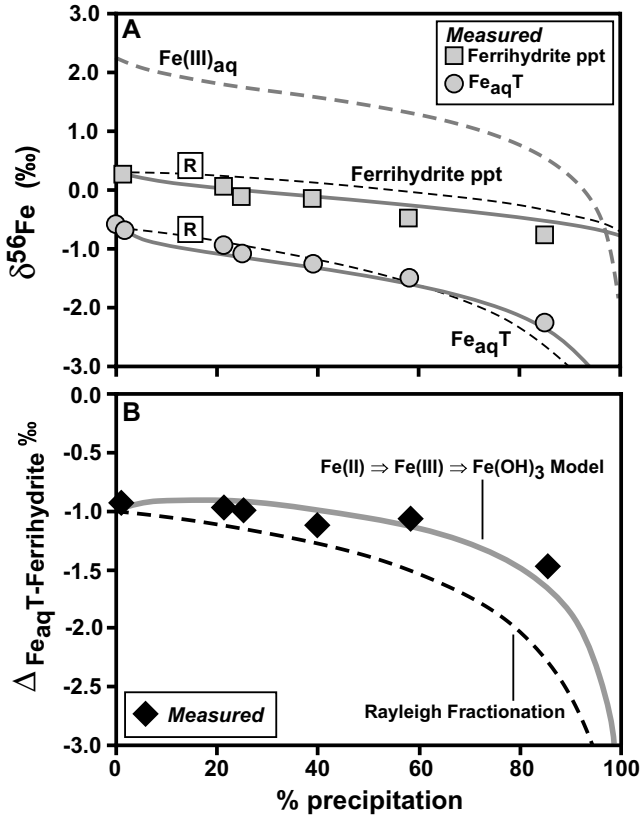

Figure 10. Fe isotope compositions for total aqueous Fe (Fe_{aq},T) and ferrihydrite (FH) precipitate and aqueous Fe-ferrihydrite fractionations from the batch oxidation and precipitation experiment of Bullen et al. (2001). (A) Measured δ^{56}Fe values from Bullen et al. (2001), compared to simple Rayleigh fractionation (short-dashed lines, noted with "R") using $10^3\ln\alpha_{Feaq\text{-}FH} = -0.9$‰, as well as the two-step re-equilibration model discussed in the text (i.e., Eqn. 12), shown in solid gray lines for the aqueous Fe and ferrihydrite components; the predicted δ^{56}Fe value for $Fe(III)_{aq}$ is shown in the heavy dashed line, which reflects continual isotopic equilibrium between $Fe(II)_{aq}$ and $Fe(III)_{aq}$. Note that in the experiment of Bullen et al. (2001), aqueous Fe existed almost entirely as $Fe(II)_{aq}$. (B) Measured fractionation between total aqueous Fe and ferrihydrite precipitate, as measured, and as predicted from simple Rayleigh fractionation (black dashed line) and the two-step model where isotopic equilibrium is maintained between aqueous $Fe(II)_{aq}$ and $Fe(III)_{aq}$ (solid gray line).

be used, and the two-step fractionation model becomes equivalent to common models such as Rayleigh fractionation, where the overall fractionation is equal to the difference of the two fractionation factors (Fig. 10). Bullen et al. (2001) noted that their data did not strictly lie along a Rayleigh fractionation curve, and hypothesized this may reflect isotopic "back exchange" between ferrihydrite and aqueous Fe. This possibility now seems unlikely, based on $Fe(III)_{aq}$-ferrihydrite exchange experiments (Poulson et al. 2003), where isotopic exchange is limited to surface sites. The two-step fractionation model discussed here is an alternative explanation for the deviation from a Rayleigh model (Fig. 10), but we cannot discount changes in the $\Delta_{Fe(III)aq\text{-}FH}$ fractionation factor with precipitation as a possibility as well.

A $Fe(III)_{aq}$-ferrihydrite fractionation of +2.0‰, as suggested by the above discussion,

seems likely to be a kinetic isotope fractionation when the rates of precipitation of the experiment of Bullen et al. (2001) are considered relative to the observations of Skulan et al. (2002), who measured a kinetic $Fe(III)_{aq}$-hematite fractionation of +1.3‰ at similar precipitation rates. That the precipitation experiment of Skulan et al. (2002) was run at 98°C, rather than at room temperature, where the Bullen et al. (2001) experiment was performed, may be one explanation for the larger inferred $Fe(III)_{aq}$-ferrihydrite fractionation, which would be expected to be larger at the lower temperature. However, it is difficult to compare these two studies directly, and it is possible that there are significant isotopic differences between hematite and ferrihydrite; Polyakov and Mineev (2000), for example, predict significant differences in $\beta_{56/54}$ factors for hematite, goethite, and lepidocrocite (Fig. 3), which remains to be tested experimentally. Fully understanding the kinetic and equilibrium fractionations involved during oxidation of $Fe(II)_{aq}$ and eventual precipitation to ferrihydrite will require experimental determination of kinetic fractionations between $Fe(III)_{aq}$ and ferrihydrite over a range of precipitation rates, as well as determination of the equilibrium $Fe(III)_{aq}$-ferrihydrite fractionation factor.

The two-step model discussed here, which is primarily motivated by the recognition that rapid isotopic exchange occurs between aqueous ferric and ferrous Fe species, contrasts with that proposed by Bullen et al (2001), who interpreted their data to reflect isotopic fractionation between ferrous Fe species such as $[Fe^{II}(OH)(H_2O)_5]^+$ and $[Fe^{II}(H_2O)_6]^{2+}$, given the rapid pathway through the ferrous Fe hydroxide species during oxidation of $Fe(II)_{aq}$. This theme was later echoed by Bullen et al. (2003), who suggested that the moderate pH experiments of Johnson et al. (2002) cannot be used to estimate the $Fe(III)_{aq}$–$Fe(II)_{aq}$ fractionation because $Fe(II)_{aq}$ is unstable at moderate pH. In reply, Johnson et al. (2003b) note that kinetic issues cannot influence the isotopic fractionation measured under equilibrium conditions, and point out that if isotopic exchange is rapid relative to the timescale of changing $Fe(II)_{aq}/Fe(III)_{aq}$ ratios in solution, isotopic equilibrium will still be maintained even if the solutions are out of chemical equilibrium. Although one might assume that as an intermediate species, $Fe(III)_{aq}$ has no effect on the overall measured Fe isotope fractionation between $Fe(II)_{aq}$ and ferrihydrite precipitate because essentially all $Fe(III)_{aq}$ is converted to ferrihydrite, this would only be true if $Fe(III)_{aq}$ was "inert" and not open to isotopic exchange, which is clearly not the case given the rapid isotopic exchange that occurs between $Fe(II)_{aq}$ and $Fe(III)_{aq}$. Consideration of the residence times of $Fe(III)_{aq}$ during oxidation of $Fe(II)_{aq}$, relative to the time required to attain isotopic equilibrium among aqueous species, indicates that, in fact, $Fe(III)_{aq}$ exerts a major control on the overall measured isotopic fractionation.

Summary observations on Fe isotope fractionation factors

A key component to developing the Fe isotope system is accurate determination of kinetic and equilibrium Fe isotope fractionation factors among a wide variety of aqueous Fe species and minerals. In the experimental systems studied to date, where equilibrium isotope fractionation factors can be confidently inferred for $Fe(III)_{aq}$–$Fe(II)_{aq}$ and $Fe(III)_{aq}$–hematite, comparison of the measured fractionations with those predicted from spectroscopic data (Polyakov and Mineev 2000; Schauble et al. 2001; Anbar et al. 2004) yields agreement in some instances but is inconsistent in others. For example, there is excellent agreement between the experimentally measured $Fe(III)_{aq}$–$Fe(II)_{aq}$ fractionation with that calculated by Anbar et al. (2004), but disagreement with Schauble et al. (2001). The greatest disparity between the two predicted fractionations lies in the reduced partition function ratio for $[Fe^{III}(H_2O)_6]^{3+}$. Use of the reduced partition function ratio for $[Fe^{III}(H_2O)_6]^{3+}$ by Anbar et al. (2004), in conjunction with that for hematite determined by Polyakov and Mineev (2000), yields a calculated $\Delta_{Fe(III)aq-hematite}$ of approximately +1.3‰ at 98°C, which is different than the measured equilibrium fractionation factor $\Delta_{Fe(III)aq-hematite}$ of -0.1 ± 0.2‰ at 98°C by Skulan et al. (2002). Considering the uncertainties in the predicted $\beta_{56/54}$ factors, however, which are

1‰ or greater at low temperature (Polyakov and Mineev 2000), this discrepancy may not be significant.

Table 2 summarizes experimentally determined Fe isotope fractionation factors for abiotic systems. These results confirm that the largest magnitude Fe isotope fractionations involve redox changes in Fe-bearing minerals and/or fluids. Many of the major Fe-bearing mineral groups (e.g., oxide, carbonate, and sulfide) have been studied to some degree, although the effect that mineralogy within a group plays has yet to be established. For example are the predicted fractionations between hematite and goethite real. The compositional effects predicted for Fe carbonates (Polyakov and Mineev 2000) have yet to be studied experimentally. Are there differences between Fe monosulfide and pyrite? It remains unknown if the differences in $Fe(II)_{aq}$–FeS and $Fe(II)_{aq}$–FeS_2 fractionations that have been experimentally determined or calculated reflect real differences, or problems with experimental and/or predicted fractionations. Finally we note that no experimental work has been conducted on Fe silicates, especially those silicates that form at low temperatures such as celadonite, whose predicted $Fe(II)_{aq}$–mineral fractionations are predicted to be significant.

Table 2. Summary of experimentally measured abiotic Fe isotope fractionation between Fe species.

Fe species	$\Delta^{56}Fe_{A\text{-}B}$	Reference
$Fe(II)_{aq}$–Fe(III) oxide	−0.9 ± 0.2	Bullen et al. (2001)
$Fe(II)_{aq}$–Hematite	−3.0 + 0.3	Skulan et al. (2002); Johnson et al. (2002); Welch et al. (2003)
$Fe(III)_{aq}$–Hematite	−0.1 ± 0.2	Skulan et al.(2002)
$Fe(II)_{aq}$–FeS	+0.3 ± 0.05	Butler et al. (2003)
$Fe(II)_{aq}$–Siderite	+0.5 ± 0.2	Wiesli et al. (2003b)
$Fe(III)_{aq}$–$Fe(II)_{aq}$	+2.9 ± 0.2	Johnson et al. (2002); Welch et al. (2003)

All results are reported for experiments conducted at room temperature (~20°C) except for $Fe(II)_{aq}$–hematite that was done at 98°C and the $Fe(II)_{aq}$–FeS which was done from 2 to 40°C.

IRON ISOTOPE VARIATIONS IN HIGH TEMPERATURE ENVIRONMENTS

Figure 11 is a histogram plot of the Fe isotope composition of high temperature rocks from the solar system. The average bulk-rock $\delta^{56}Fe$ value of 43 terrestrial igneous rocks is 0.00 ± 0.05‰ (on an IRMM-014 scale, the $\delta^{56}Fe$ of igneous rocks averages +0.09 ± 0.05‰), and there is no correlation between Fe isotope compositions and bulk-rock chemical compositions. For example, silicic continental volcanic and plutonic rocks have the same isotopic composition as oceanic and continental basalts. Lunar rocks define a range of Fe isotope compositions that is similar to those of terrestrial igneous rocks (Fig. 11). In contrast, the lunar regolith has higher $\delta^{56}Fe$ values as compared to those of crystalline lunar rocks (Fig. 11), which probably reflects space weathering processes and Fe loss during vaporization (Wiesli et al. 2003a; see below). The HED meteorite group (Howardites, Eucrites, Diogenites) define a range of Fe isotope composition that is similar to that of terrestrial samples (Fig. 11; Mullane et al. 2003c), although Poitrasson et al. (2002) suggests that Eucrites are skewed to lower $\delta^{56}Fe$ values by ~0.05‰. Metal from Iron meteorites has the same isotopic composition as terrestrial igneous rocks, where the average $\delta^{56}Fe$ value of 10 analyzed Iron meteorites is −0.03 ± 0.04‰ (Zhu et al. 2001; Kehm et al. 2003). In contrast, Pallasites (stony iron meteorites) have a wide range in isotopic compositions (Fig. 11; $\delta^{56}Fe$ from approximately −1.0 to +0.1‰) as measured in Fe metal and silicates (Zhu et al. 2001, 2002; Mullane et al. 2002; Kehm et al. 2003). It is

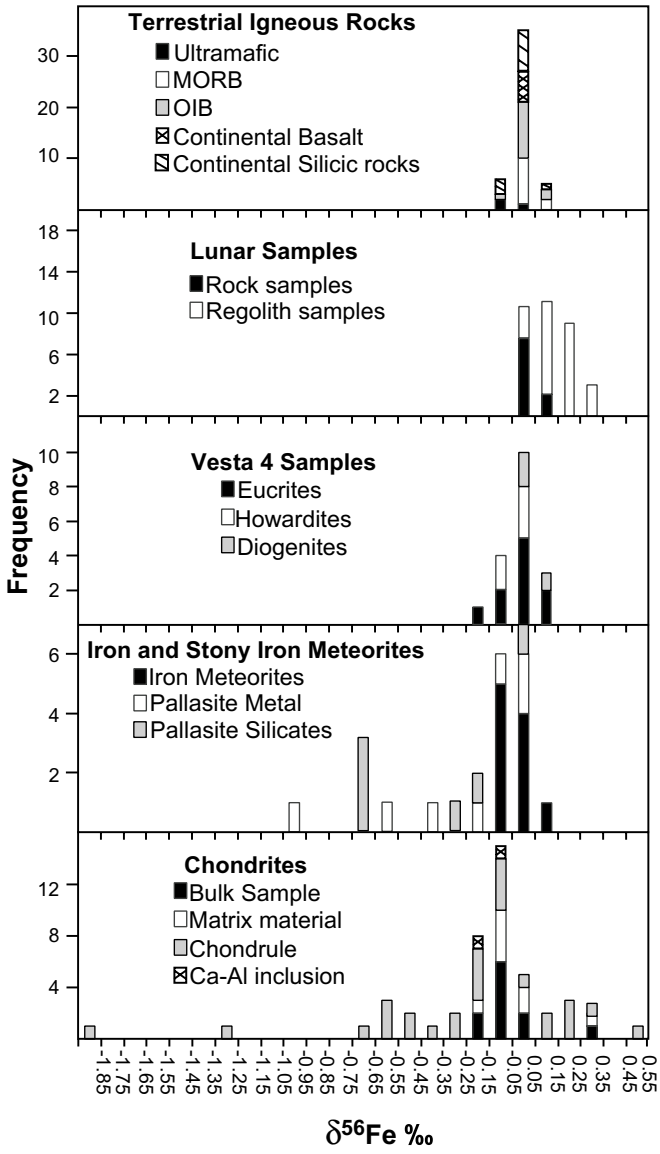

Figure 11. Frequency diagram of Fe isotope compositions measured in igneous rocks from terrestrial and extraterrestrial samples. The bin range is 0.1‰ in δ^{56}Fe values, which is the typical external precision (2σ) of an Fe isotope measurement. The data summarized in the diagram includes Fe isotope analyses from four laboratories and inter-laboratory bias has been corrected by normalization to a constant δ^{56}Fe value of –0.09‰ for IRMM-014, which places Fe isotope variations relative to the average of terrestrial igneous rocks (e.g., Beard et al. 2003b). Data sources are: terrestrial igneous rocks from Beard et al. (2003b); lunar rock and regolith samples from Wiesli et al. (2003a) HED meteorite data from Zhu et al. (2001), and Mullane et al. (2003c); Iron and Pallasite meteorite data from Zhu et al. (2001), Mullane et al. (2002), and Kehm et al. (2003); chondrite meteorite data from Zhu et al. (2001), Mullane et al. (2003a; b), and Kehm et al. (2003).

unknown if the wide range in isotopic compositions of Pallasites is due to high-temperature fractionation between Fe metal and silicate minerals (see below) or oxidation by vapors that are produced during crystallization of silicate liquids (e.g., Wasson and Choi 2003).

The largest variations in Fe isotope compositions occur in chondrites (Fig. 11). For example, individual chondrules define a range in δ^{56}Fe values from −1.9 to +0.5‰ (Zhu et al. 2001; Kehm et al. 2003; Mullane et al. 2003a,b). Bulk chondritic meteorites define a significant range in Fe isotope compositions, where 8 bulk chondritic meteorites vary from δ^{56}Fe values of −0.24 to +0.29‰ (Zhu et al. 2001; Kehm et al. 2003; Fig. 11). The matrix material in chondritic meteorites is also variable where δ^{56}Fe varies from −0.15 to +0.34‰ (Zhu et al. 2001; Mullane et al. 2003b; Fig. 11). Two bulk calcium aluminum inclusions (CAI) have been measured in chondrites and these have Fe isotope compositions that are similar to the matrix material analyzed in the same meteorite (Mullane et al. 2003a,b).

The Fe isotope variations measured in these terrestrial and extraterrestrial samples were all produce by mass-dependent processes, and it appears that the solar nebula was well homogenized with respect to variations in ^{54}Fe, ^{56}Fe, ^{57}Fe, and ^{58}Fe (Zhu et al. 2001; Kehm et al. 2003). This stands in marked contrast to the O isotope compositions of extraterrestrial materials, where different meteorite groups tend to have unique ^{17}O/^{16}O–^{18}O/^{16}O variations, including incomplete mixing with extrasolar ^{16}O-rich components. The only non-mass-dependent Fe isotope variations that have been reported for extraterrestrial samples are parts of some CAIs from chondritic meteorites, where there appears to be an excess of ^{58}Fe that likely reflects nucleosynthesis processes (Völkening and Papanastassiou 1989). In the one high precision Fe isotope study that made ^{54}Fe, ^{56}Fe, and ^{58}Fe isotope analyses in a manner that preserved natural, mass-dependent variations (Kehm et al. 2003), these workers found that all variations in bulk chondrites and individual chondrules are associated with mass-dependent processes. It appears that evidence for non-mass dependent Fe isotope variations can only be found in the most refractory portions of the oldest extraterrestrial materials (e.g., Völkening and Papanastassiou 1989; Birck 2004), or perhaps in presolar grains (Clayton 1999).

The range in δ^{56}Fe values in bulk chondrites and chondrite matrices is though to reflect alteration processes that occurred on the chondritic parent bodies, probably through interaction with aqueous solutions (Kehm et al. 2003). Of particular significance is the composition of the bulk analysis of the chondritic meteorite Orgueil. Both Zhu et al. (2001) and Kehm et al. (2003) have analyzed aliquots from this sample and the analysis by Zhu et al. (2001) is the only bulk chondrite that has a positive δ^{56}Fe value (+0.29‰); however, the aliquot analyzed by Kehm et al. (2003) had a δ^{56}Fe of −0.04‰, a value that is similar to the 7 other bulk chondrites that have been analyzed. This contrast does not appear to be an analytical artifact, since both studies analyzed bulk samples of Murchison and Allende, and the reproducibility between the two labs is good. The different isotopic compositions analyzed by both labs for the Orgueil meteorite is inferred to be a result of fine-scale heterogeneities in the meteorite. Mullane et al. (2003a,b) consider the similar Fe isotope compositions of aliquots of matrix material and CAI from the Allende meteorite to be evidence for redistribution of Fe because CAIs have exceedingly low Fe contents.

The 2.5‰ range in ^{56}Fe/^{54}Fe ratios of chondrules is interpreted to reflect evaporation and condensation during chondrule formation, alteration processes, and initial isotopic heterogeneities in the source materials. Iron isotope analyses conducted by ion microprobe on olivine from Chainpur chondrules place some constraints on possible Fe evaporation models during chondrule formation (Alexander and Wang 2001). Rapid calculated cooling rates are required to produce minimal Fe isotope fractionation, and these agree well with cooling rates inferred from experiments that produce the petrographic textures which are found in chondrules. The precision of individual Fe isotope analyses, however, were ~2‰ in ^{57}Fe/^{56}Fe, and were not sufficient to satisfactorily resolve distinct differences in Fe isotope compositions.

Based on high-precision $^{56}Fe/^{54}Fe$ ratios determined for 8 chondrules from the ordinary chondrite Tieschitz, Kehm et al. (2003) concluded that there was no evidence for positive $\delta^{56}Fe$ values relative to terrestrial igneous rocks. The lack of evidence for heavy Fe isotope compositions led Kehm et al. (2003) to conclude that evaporative loss of Fe was minimal, or if evaporation occurred it did not proceed via Rayleigh process. Instead, Kehm et al. (2003) suggest that the trend of Fe isotope compositions in chondrules that have negative $\delta^{56}Fe$ values is better explained by loss of Fe during condensation processes, assuming that gas and condensate do not maintain equilibrium. In another high-precision Fe isotope study of individual chondrules from the Allende and Chainpur chondritic meteorites, Mullane et al. (2003a,b) concluded that the limited Fe isotope variations in chondrules rules out Rayleigh evaporation processes. Mullane et al. (2003a,b) also highlight the lack of correlation between Fe isotope composition and chondrule size and texture, suggesting that mass-dependent isotopic heterogeneities in the chondrule starting materials is the most likely explanation for the range in Fe isotope compositions. Secondary processes are likely to homogenize Fe isotope compositions between matrix, chondrules, and CAI, and it is possible that initial isotopic variability in the solar nebula was much greater.

There may be some subtle differences in the Fe isotope composition of different planetary bodies. For example, the average $\delta^{56}Fe$ value of bulk chondritic meteorites is $-0.11 \pm 0.07‰$, excluding the Orgueil analysis by Zhu et al. (2001; see above). Poitrasson et al. (2002) has noted that the SNC and HED meteorite groups have $\delta^{56}Fe$ values that are slightly lower than terrestrial igneous rocks, approximately −0.07‰, where as they note that lunar rocks have slightly higher $\delta^{56}Fe$ values that are 0.06‰ greater than terrestrial rocks. The similarity between SNC and HED and the average of chondritic meteorites, and the slightly higher $\delta^{56}Fe$ of the Earth-Moon system is interpreted as evidence for vaporization and loss of Fe from the Earth-Moon system during formation of the moon by a giant impactor (Poitrasson et al. 2002). The isotopic differences between the Earth-Moon system and the SNC and HED parent bodies, however, are near the limit of analytical precision, and these interpretations may change as the database is expanded. For example, using a different suite of lunar samples, Wiesli et al. (2003a) determined that the average $\delta^{56}Fe$ value of 9 lunar rock samples was $0.03 \pm 0.05‰$, and individual samples varied from −0.04 to +0.13‰. Similarly, in a more extensive Fe isotope survey of HED meteorites (5 Howardites, 9 Eucrites and 3 Diogenites), Mullane et al. (2003c) observed that there are no Fe isotope differences between Howardites, Eucrites, and Diogenites, and that the average $\delta^{56}Fe$ value of the HED meteorites analyzed by Mullane et al. (2003c) is $-0.01 \pm 0.06‰$. Iron meteorites, which presumably represent material from differentiated planets, have an average $\delta^{56}Fe$ of $-0.03 \pm 0.04‰$ for the 10 analyzed samples. In summary, based on the current data set, it is difficult to determine if different planets have resolvable differences in their Fe isotope composition, or if these planets have compositions that are unique relative to bulk chondrites. An important avenue for further study would be measurement of the isotopic compositions of elements of different volatility, including Fe, which may provide more robust constraints on accretion history of planetary bodies.

Fe isotope fractionation produced by vaporization

Loss of Fe during vaporization processes can lead to significant Fe isotope fractionation in a variety of environments. For example, deep sea iron spherules (micro iron meteorites) have $\delta^{56}Fe$ values that are up to +40‰ greater than the average of terrestrial igneous rocks and iron meteorites (Herzog et al. 1999). The isotopic compositions of Cr and Ni in deep sea spherules are similarly enriched in the heavy isotope relative to an average terrestrial value. These extreme isotopic compositions suggest that up to 95% of the Fe in the spherule was lost by evaporation and heating during passage through the Earth's atmosphere. Similar fractionations are produced in thermal ionization mass spectrometry, when Fe isotope analysis during heating results in the preferential loss of the light isotopes (Beard and Johnson 1999).

Vaporization processes that produce the high δ^{56}Fe values of deep sea spherules are, of course, more complicated, because a large portion of the heating and vaporization occurs in the atmosphere, and is accompanied by conversion of Fe metal to Fe oxides.

Vaporization and loss of Fe is the preferred explanation for the high δ^{56}Fe values measured in the lunar regolith, as compared to lunar rock samples (Wiesli et al. 2003a). The lunar regolith is formed by space weathering processes that produce changes in the primary mineralogy of crystalline rocks, largely through production of agglutinitic glass fragments and formation of regolith that is primarily controlled by micrometeorite impacts and solar wind sputtering processes (e.g., Keller and McKay 1993; Bernatowicz et al. 1994; Hapke et al. 1994; Hapke 2001). During formation of agglutinitic glass, nano-phase Fe metal is produced which has a strong influence on the magnetic properties of regolith as measured by I_S values (ferromagnetic resonance intensity; Morris 1976). High I_S values are correlated to a high proportion of nano-phase Fe metal. The relative exposure age of regolith to space weathering processes is measured using the I_S/FeO ratio (I_S values are normalized to the soil's total Fe in order to normalize for differences in bulk composition), where values of 30 and 60 delineate immature from submature, and submature from mature, respectively (Morris 1976). Within an individual soil sample, the finest fractions have the highest I_S/FeO values and the highest agglutinitic glass proportion (Taylor et al. 2001), and the finest size fractions have a greater proportion of nano-phase Fe metal relative to coarser size fractions.

Immature soil samples have δ^{56}Fe values that are indistinguishable from lunar rocks, whereas submature and mature soils have δ^{56}Fe values that are greater than those of lunar rocks, and δ^{56}Fe values are positively correlated with I_S/FeO values (Fig. 12). Lunar regolith samples in general tend to have heavy isotopic compositions as compared to lunar rock samples, as demonstrated by isotopic analyses of O, Si, S, Mg, K, Ca, and Cd (Epstein and Taylor 1971; Clayton et al. 1974; Russell et al. 1977; Esat and Taylor 1992; Humayun and Clayton 1995; Sands et al. 2001; Thode 1976). The origin of isotopic compositions that are enriched in the heavy isotopes has been presumed to reflect sputtering by solar wind and vaporization, where preferential loss of the lighter isotope to space occurs. In contrast to previous isotopic studies, the Fe isotope compositions measured in the Lunar Soil Characterization Consortium samples can be related to a specific phase based on the positive correlation in I_S/FeO and δ^{56}Fe values (Fig. 12).

High-temperature inter-mineral Fe isotope fractionation

The calculated Fe isotope fractionation factors of Polyakov and Mineev (2000) indicate that at high temperatures (>500°C) there may be analytically resolvable (e.g., 0.1‰ in ^{56}Fe/^{54}Fe) inter-mineral fractionations between magnetite and olivine and between clinopyroxene and olivine (Fig. 13). Berger and von Blanckenburg (2001) reported magnetite-silicate fractionations for metamorphic rocks that were consistent with the calculated values of Polyakov and Mineev (2000), although these workers suggested that Fe isotope fractionation was more strongly controlled by changing redox conditions as opposed to temperature dependency. Zhu et al. (2002) reported significant high-temperature, inter-mineral isotope fractionation based on analyses of 3 spinel peridotite mantle xenoliths, where olivine has δ^{56}Fe values that are ~0.2‰ lower than coexisting clino- and orthopyroxene, and concluded that these inter-mineral fractionations were a result of high-temperature equilibrium isotopic exchange (Fig. 13). Similar Fe isotope compositions measured on minerals from spinel peridotite were reported by Williams et al. (2002). In addition to the inter-mineral Fe isotope differences measured in spinel peridotites, Zhu et al. (2002) reported that olivine from two Pallasite meteorites has δ^{56}Fe values that are 0.14 and 0.19‰ lower than coexisting Fe metal (Fig. 13).

In contrast to the above findings, which suggest that there are equilibrium high-temperature inter-mineral fractionations, Mullane et al. (2002) reported that silicate minerals

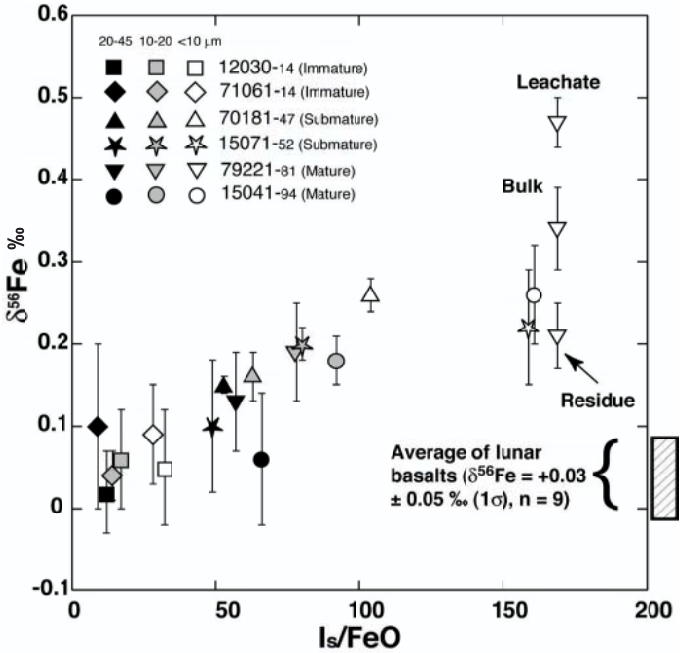

Figure 12. Plot of I_s/FeO versus δ^{56}Fe values of lunar regolith samples from the Lunar Soil Characterization Consortium. The sub-scripted numbers after the sample numbers are the I_s/FeO values measured for the <250 μm sized fraction. All analyses are for bulk samples of the different sized fractions; error bars are 2σ as calculated from 2 or more complete Fe isotope analyses. Modified from Wiesli et al. (2003a).

in Pallasites are homogenous in Fe isotope composition, and that coexisting Fe metal in some samples has a δ^{56}Fe value that is greater than the silicate mineral and in other samples the Fe-metal has a δ^{56}Fe that is less than the coexisting silicate mineral. Beard and Johnson (2004) analyzed coexisting olivine, clinopyroxene, and orthopyroxene from 8 spinel peridotite mantle xenoliths and found that there was not a significant Fe isotope fractionation between orthopyroxene and olivine (Fig. 13). Clinopyroxene-olivine fractionations for all but one sample were insignificant as well (Fig 13). Beard and Johnson (2004) noted that the measured Fe isotope differences between clinopyroxene and olivine were a function of Fe isotope composition as shown on a δ-δ plot (Fig. 14). The negative correlation between $\Delta^{56}Fe_{cpx\text{-}ol}$ and the δ^{56}Fe value of olivine (or clinopyroxene) is interpreted to be a result of open-system processes, drawing on analogous relations that have been observed in oxygen isotope studies (e.g., Gregory and Criss 1986). Specifically, Beard and Johnson (2004) hypothesized that metasomatic alteration by a fluid that had a low δ^{56}Fe value coupled with differences in the relative Fe diffusion rates of olivine, orthopyroxene, and clinopyroxene, may produce the trends in δ^{56}Fe values measured in mantle minerals.

Beard and Johnson (2004) also investigated Fe isotope fractionation between magnetite and silicate minerals in 4 volcanic rocks from Mt. Lassen, California. In these samples there was no resolvable difference in Fe isotope composition between magnetite, olivine, amphibole, and biotite, and all the minerals had δ^{56}Fe values that overlapped with the Fe isotope composition of igneous rocks. These results stand in contrast to the findings of Berger and von Blanckenburg (2001), who analyzed magnetite and silicate minerals from slowly cooled metamorphic rocks and found significant differences between their Fe isotope

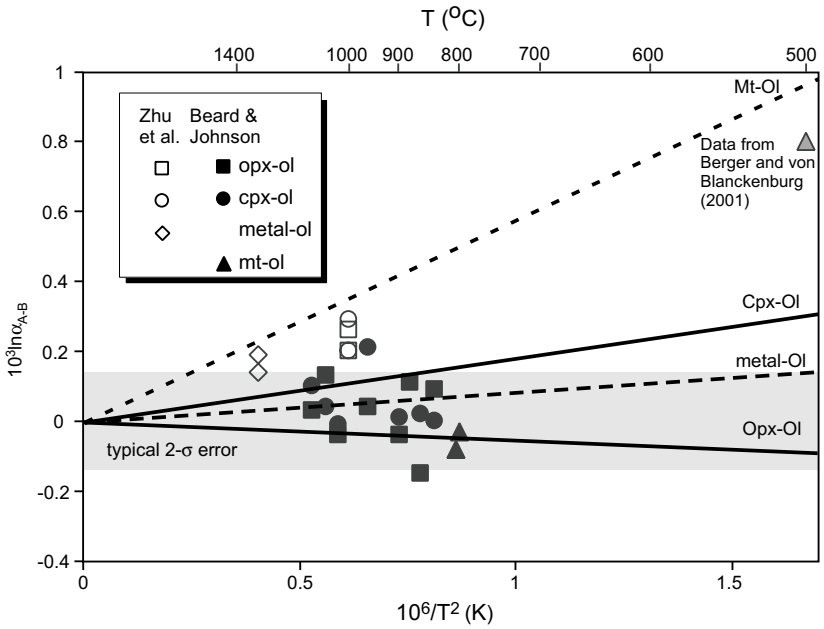

Figure 13. Plot of $10^3 \ln\alpha_{A-B}$ values versus $10^6/T^2$ (T in K) for inter-mineral fractionation between magnetite-olivine, orthopyroxene-olivine, and clinopyroxene-olivine, and Fe metal-olivine as calculated from spectroscopic data by Polyakov and Mineev (2000), and as measured from natural samples by Zhu et al. (2002), Beard and Johnson (2004). Also shown is the Fe isotope fractionation factor between magnetite and Fe-silicates measured by Berger and von Blanckenburg (2001).

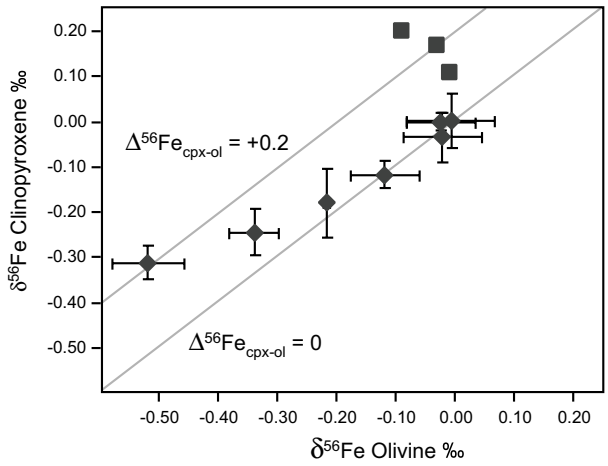

Figure 14. Inter-mineral Fe isotope fractionations among olivine and clinopyroxene from spinel peridotite mantle xenoliths. Data are from Zhu et al. (2002) (■) and Beard and Johnson (2004) (◆). In the study by Beard and Johnson (2004), the difference in the Fe isotope composition between clinopyroxene and olivine is larger as a function of their δ^{56}Fe values, suggesting disequilibrium fractionation.

compositions. The differences in Fe isotope fractionation between magnetite and silicate minerals analyzed in these two studies may reflect differences between the cooling rates of the samples. For example, open-system isotopic exchange between magnetite and silicates may have taken place during the slow cooling of the metamorphic rocks analyzed by Berger and von Blanckenburg (2001), whereas the rapidly cooled volcanic rocks would have been resistant to such open system behavior.

Iron isotope fractionation between garnet and clinopyroxene was measured for coexisting mineral pairs from 4 eclogites, 2 garnet peridotites and 1 garnet pyroxenite (Beard and Johnson 2004). Garnets have δ^{56}Fe values that range from −0.39 to +0.01‰, and clinopyroxenes have δ^{56}Fe values that range from −0.03 to +0.30‰ (Fig. 15). The Fe isotope compositions of coexisting garnet and clinopyroxene are positively correlated, and six of the seven samples have $\Delta^{56}Fe_{cpx\text{-}gt}$ of approximately +0.3‰, whereas the garnet pyroxenite sample has a significantly lower $\Delta^{56}Fe_{cpx\text{-}gt}$ fractionation of 0.07‰. Mass-balance calculations using the measured Fe contents and isotope compositions, as well as visually estimated modal proportions of garnet and clinopyroxene, indicate that the bulk Fe in these samples range from −0.10 to +0.07‰, in excellent agreement with analyzed bulk-rock Fe isotope analyses. Based on the Fe isotope variations between garnet and pyroxene on a δ-δ plot, Beard and Johnson (2004) inferred that there is resolvable high-temperature inter-mineral fractionation between garnet and pyroxene.

Perhaps the most surprising result of these mantle mineral studies is that the mantle has heterogeneities of 0.5‰ in δ^{56}Fe values (Fig. 14). These isotopic heterogeneities stand in marked contrast to the isotopic homogeneity of igneous rocks in oceanic and continental environments. Therefore it is believed that isotopically anomalous mantle is minor in abundance, and any contribution to basaltic melts must be small. Additionally, because there are no significant Fe isotope fractionations among the major Fe-bearing minerals (silicates and oxides) that are common liquidus phases in crustal magmas, the isotopic homogeneity recorded in basaltic magmas will be retained during differentiation. We are therefore left with the conclusion that although significant Fe isotope variability may be produced in parts of the mantle, such variability may be "left in the mantle" during magma genesis, and significant Fe

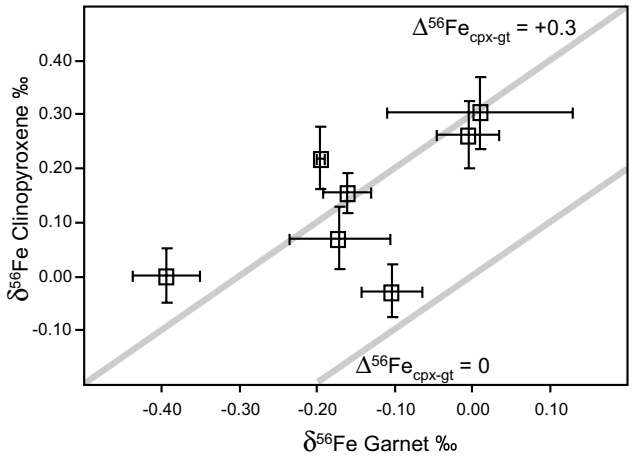

Figure 15. δ^{56}Fe of garnet versus that of coexisting clinopyroxene for eclogites, garnet peridotites, and garnet pyroxenite. Six of the seven samples scatter about a $\Delta^{56}Fe_{cpx\text{-}gt}$ of +0.3‰ over a wide range in δ^{56}Fe values measured in the minerals. Error bars are 1-SD of the mean as determined by two or more replicate analyses of the mineral. Modified from Beard and Johnson (2004).

isotope fractionations only re-appear in natural systems in surface environments where low-temperature fractionations between fluids minerals occurs, as well as biological cycling of Fe.

IRON ISOTOPE VARIATIONS IN LOW TEMPERATURE ENVIRONMENTS

The homogenous Fe isotope composition of igneous rocks ($\delta^{56}Fe = 0.00 \pm 0.05‰$, 1σ; Fig. 1; Beard et al. 2003b) suggests that the continents and oceanic crust formed with a $\delta^{56}Fe$ value of zero, providing a baseline with which to compare Fe isotope variations in low-temperature environments. Aeolian deposits, such as loess and modern aerosol particles, and fluvial sediments, such as modern oceanic turbidites and the suspended load from rivers, have homogenous Fe isotope compositions, similar to that of igneous rocks (Fig. 16). Low organic-carbon (C_{org}) grey shales from the Proterozoic and Phanerozoic are slightly more variable in Fe isotope composition where $\delta^{56}Fe = -0.36$ to $+0.39‰$, but all of these clastic sedimentary rocks have a normal distribution of Fe isotope compositions whose average is the same as that of terrestrial igneous rocks. (Fig. 16). In contrast to the homogenous Fe isotope composition of these organic-poor clastic sediments, black shales ($C_{org} > 0.5$ wt%) define a wide range of Fe isotope compositions, ($\delta^{56}Fe = -2.28$ to $+0.64‰$; Fig. 16). In addition to the significant Fe isotope variations recognized in C_{org}-rich shales, there are even larger variations in chemically precipitated sediments that formed at low temperatures. Pliocene to Recent Fe-Mn crusts from the North Atlantic Ocean and the Pacific Ocean typically have Fe isotope compositions that are shifted to lower $\delta^{56}Fe$ values as compared to igneous rocks (Fig. 16). Similarly, hydrothermal vent fluids from Mid-Ocean Ridges (MOR) have $\delta^{56}Fe$ values that are shifted to lower values as compared to terrestrial igneous rocks. Late Archean to Early Proterozoic Banded Iron Formations (BIFs) define a significant range of Fe isotope compositions from -2.5 to $+1.1‰$. The large Fe isotope variations recorded in BIFs are generally correlated with the mineralogy of individual BIF layers (Johnson et al. 2003a), where $\delta^{56}Fe$ values increase in the order pyrite-Fe carbonate-oxides (Fig. 16). These isotopic differences may be related to equilibrium Fe isotope fractionations that are intrinsic to specific minerals, reflecting precipitation or diagenetic reactions that occurred in relation to biotic processing of Fe.

Fe isotope variations in clastic sediments

The very restricted range in Fe isotope compositions of low-C_{org} clastic sedimentary rocks is quite remarkable considering the fact that these samples have been extensively processed through the sedimentary rock cycle, including mechanical and chemical weathering of pre-existing rock, sedimentary transport by wind and water, and deposition, diagenesis, and lithification. Low-temperature surficial processes that involve weathering and transport, diagenesis, and lithification of sediments produce some of the largest variations in light stable isotope compositions (e.g., H, C, and O). The large range in H, C, and O isotope compositions of such materials is partly a function of the fact that isotopic fractionations are large at low temperatures, but also reflects the complex interactions that take place between fluids and rocks, where significant reservoirs of H and O, for example, may exist in both fluids and minerals. The $\delta^{18}O$ values of sediments are much more variable ($+10$ to $+30‰$; Arthur et al. 1983) than those of fresh igneous rocks (e.g., Eiler 2001); the majority of oxygen isotope variation in igneous rocks is attributed to variable amounts of mixing between juvenile igneous sources that have a homogenous oxygen isotope composition with crustal material that has experienced surface alteration processes (see Eiler 2001 for a review). The roles that low temperature surficial processes have in controlling Fe isotope variations are largely unknown, but based on the similar range of $\delta^{56}Fe$ values that clastic sediments and igneous rocks share, it would appear that surficial processes that occur under at least oxic conditions do not significantly change the Fe isotope composition of bulk clastic sedimentary rocks.

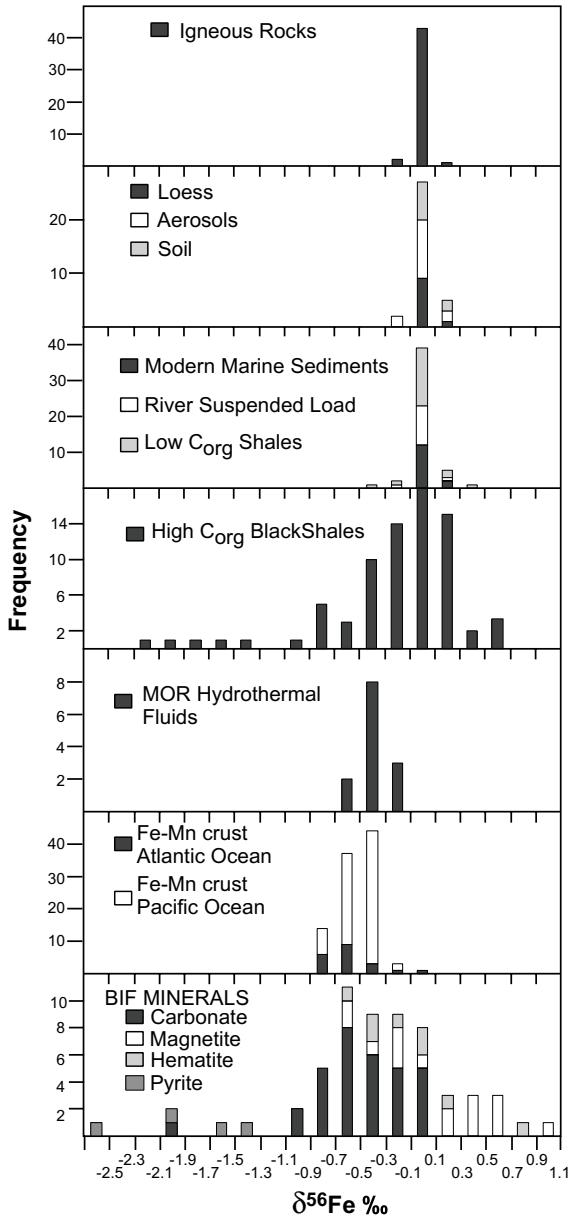

Figure 16. Frequency diagram of Fe isotope compositions measured in igneous and sedimentary rocks and MOR fluids. Inter-laboratory bias in Fe isotope measurements has been corrected by normalizing to a δ^{56}Fe value of −0.09‰ for the IRMM-014 standard, which places Fe isotope measurements relative to the average of terrestrial igneous rocks. Data sources are: terrestrial igneous rocks from Beard et al. (2003b); aeolian sediments and rocks from Beard et al. (2003a); fluvial low-C_{org} sediments and rocks from Beard et al. (2003a), high-C_{org} black shales from Yamaguchi et al. (2003) and Matthews et al. (2004); hydrothermal fluids from Sharma et al. (2001) and Beard et al. (2003a); Atlantic Ocean Fe-Mn crust data from Zhu et al. (2000), Pacific Ocean Fe-Mn crust data from Chu et al. (2003); Banded Iron Formations from Johnson et al. (2003a).

The significant difference in the relative behavior of Fe and O isotopes for clastic sedimentary rocks in part reflects the redox behavior of Fe. Iron solubility is highly dependent on redox state, where for example, in neutral pH oxic environments, the solubility of Fe is so low that significant transport of aqueous Fe is precluded. If Fe is not partitioned into different reservoirs, no isotopic variability will be produced in bulk samples. However for O isotopes, in fluid-rock systems there is typically sub-equal amounts of O in the two components, so that even at moderate fluid to rock ratios the bulk composition of the rock can be shifted toward the isotopic composition of the fluid, and vice versa. In contrast the quantity of Fe that is dissolved in oxic fluids is very low, and therefore it will be relatively difficult to shift the Fe isotope composition of a rock through fluid-rock interactions in an oxygenated environment. Moreover, Fe typically behaves as a conservative element during weathering (e.g., Canfield 1997) in oxic environments where, for example, nearly all Fe transported by rivers is contained in the suspended and bed loads and very little occurs in the dissolved load. Therefore, even if there are isotope fractionations associated with weathering of silicates and the production of Fe oxides and oxyhydroxides from aqueous Fe solutions, it is anticipated that there will be minimal net isotope shift in the bulk sample because Fe is not easily separated into different pools.

The δ^{56}Fe values of igneous rocks and suspended river loads are compared to the modal fraction of ferric oxide/hydroxide in suspended river loads in Figure 17. Despite markedly higher ferric oxide/hydroxide contents produced during weathering, the range in δ^{56}Fe values of bulk suspended river loads overlaps that of igneous rocks. Moreover, because there does not appear to be differences in the isotopic compositions of oxides and various silicate minerals in igneous rocks, suggesting that differential weathering is unlikely to produce significant Fe isotope variability. It is possible, however, that weathering in the presence of organic ligands will produce Fe isotope fractionations (Brantley et al. 2001). It remains unclear if Fe in poorly crystalline or labile components in suspended river loads is isotopically variable, or if the dissolved load of Fe is isotopically distinct from bulk crustal sources, and this is an important future avenue of research. Iron isotope variations have been measured in some extreme chemical weathering environments, as shown by analysis of highly altered oceanic crust where 80% of the Fe has been mobilized from the basaltic crust through interaction with mid-ocean ridge fluids, followed by production of ferric iron-rich clays like celadonite,

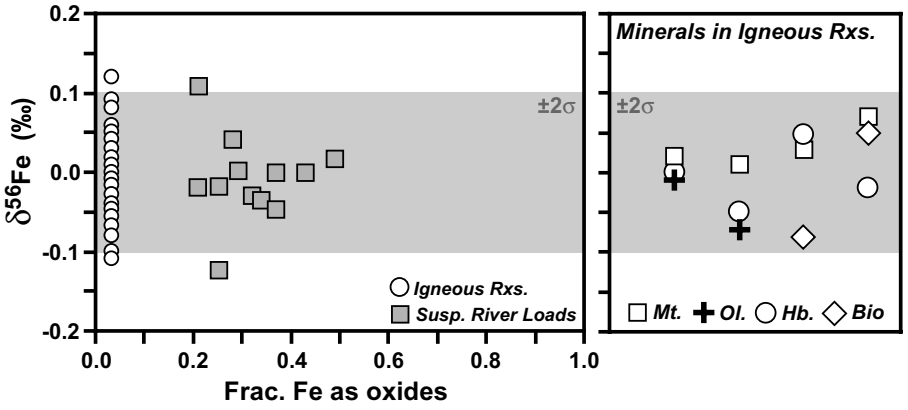

Figure 17. Comparison of δ^{56}Fe values for bulk igneous rocks (○), suspended river loads (■) and individual minerals from volcanic rocks (right panel). Left panel shows the fraction of Fe that exists as oxides (data for igneous rocks arbitrarily plotted as 0.02). Right panel shows δ^{56}Fe values for coexisting magnetite (□), olivine (✚), hornblende (○), and biotite (◇) in four volcanic rocks. Data from Canfield (1997), Beard et al. (2003a), and Beard and Johnson (2004).

leaving behind an altered basaltic crust that has high δ^{56}Fe values relative to unaltered basalt (e.g., Rouxel et al. 2003; see below).

The variability of Fe isotope compositions in black shales seems likely to reflect redox cycling of iron in anoxic environments. Reductive processes may include bacterial iron reduction or interaction with H_2S or other reducing agents, and if Fe is separated into isotopically distinct reservoirs, Fe isotope variations may be recorded in bulk samples. Bacterial iron reduction produces $Fe(II)_{aq}$ that has low δ^{56}Fe values (Johnson et al. 2004), and $Fe(II)_{aq}$ in equilibrium with $Fe(III)_{aq}$ will also have low δ^{56}Fe values (Johnson et al. 2002; Welch et al. 2003). Preliminary Fe isotope analyses of pore fluids from C_{org}-rich sediments indicate that the $Fe(II)_{aq}$ has a low δ^{56}Fe value, as low as −5‰ (Severmann et al. 2002), consistent with the expectation that reduced species should have relatively low δ^{56}Fe values. An additional pathway that may produce Fe isotope variability is precipitation of diagenetic siderite and iron sulfides. Initial experimental studies suggest that siderite and Fe monosulfide should have δ^{56}Fe values that are low relative to $Fe(II)_{aq}$ (Table 2). Empirical studies agree with these experiments. For example, an Fe isotope investigation of the Kimmeridge Clay Formation (a C_{org}-rich sequence of shales and mudstones, and carbonate material) concluded that mudstones that contain pyrite and siderite tend to have δ^{56}Fe values that are up to 0.6‰ lower than dolostones from the same formation (Matthews et al. 2004). Moreover, Matthews et al. (2004) demonstrated that pyrite from sedimentary sequences tends to have δ^{56}Fe that are ~0.4‰ less than the Fe isotope composition of most lithologic Fe, based on analysis of pyrite nodules and pyritized ammonites. Similarly low δ^{56}Fe values for pyrite were found in black shales that are interbedded with banded iron formation (Johnson et al. 2003). Another study of Archean-age black shales highlighted that magnetite-rich samples have very low δ^{56}Fe values (as low as −2.3‰), and may be explained by dissimilatory Fe(III) reducing bacteria, providing evidence for the ancient origin of Fe metabolism (Yamaguchi et al. 2003). The Fe isotope fractionations that may be produced during biological processing, and possible examples from the rock record, are discussed in the next chapter (Johnson et al. 2004).

Fe isotope variations in MOR hydrothermal fluids

Mid-Ocean Ridge (MOR) hydrothermal fluids have distinctly lower δ^{56}Fe values as compared to terrestrial igneous rocks and low-C_{org} clastic sedimentary rocks; thirteen analyses of vent fluids from the Atlantic and Pacific oceans define a range in δ^{56}Fe from −0.69 to −0.21‰ with an average of -0.39 ± 0.13‰ (Sharma et al. 2001; Beard et al. 2003a). Sharma et al. (2001) speculated that the origin of the low δ^{56}Fe values in MOR hydrothermal vent fluids is a product of 1) complex leaching reactions of basalts by fluids, 2) precipitation of sulfides from vent fluids, and 3) phase separation between vapor and brine solutions. At the time, it was not possible to evaluate all of these ideas because of sparse data, and poor precision for some samples (±0.04–0.68‰). More recent studies that include high-precision data on 1) MOR hydrothermal fluids that include analyses of brine and vapor from the same vent (Beard et al. 2003a), 2) sulfide deposits from a MOR spreading center (Rouxel et al. 2004), and 3) altered oceanic crust (Rouxel et al. 2003) allows some of these ideas to be evaluated.

Vapor and brine from the Brandon vent of the East Pacific Rise have identical Fe isotope compositions, implying that phase separation does not produce an isotopic fractionation (Beard et al. 2003a). The role that sulfide precipitation plays in controlling the Fe isotope composition of the fluid remains unknown. The precision of the two sulfide analyses reported by Sharma et al. (2001) was not sufficient to resolve if sulfide precipitation would produce Fe isotope fractionation in the vent fluid. In a detailed study of sulfides from the Lucky Strike hydrothermal field from the mid Atlantic Ridge, however, Rouxel et al. (2004) found that sulfides span a range in δ^{56}Fe values from −2.0 to +0.2‰, and that pyrite/marcasite has lower δ^{56}Fe values (~1‰) as compared to chalcopyrite. The variations in mineralogy and isotope composition are inferred to represent open-system equilibrium fractionation of Fe whereby

chalcopyrite (a high-temperature sulfide) precipitated from fluids, producing a residual fluid that had low δ^{56}Fe values. Pyrite that precipitated from lower temperature fluids are thought to be the explanation for the relatively low δ^{56}Fe values measured for pyrite. So far, the evidence seems to support sulfide precipitation from hydrothermal fluids as a means to produce solutions that have low δ^{56}Fe values. Additional data on vent fluid-sulfide chimney pairs indicate that the sulfides are 0.1–0.3‰ higher in ^{56}Fe/^{54}Fe ratios as compared to the matching vent fluid (S. Severmann, et al., unpublished data). These empirically measured sulfide-aqueous Fe fractionation factors are consistent with the direction of Fe isotope fractionation inferred by Rouxel et al (2004), but they are smaller by a factor of 2 or more.

Fluid-rock interactions during hydrothermal alteration are also inferred to produce fluids that have low δ^{56}Fe values. In a survey of the Fe isotope composition of oceanic crust from ODP site 801C Rouxel et al. (2003) found that the basaltic crust is heterogeneous in its Fe isotope composition, and that δ^{56}Fe values in altered crust increase with increasing degrees of Fe leaching. Rouxel et al. (2003) inferred these variations to reflect kinetic isotopic fractionations that were associated with Fe leaching, or alternatively formation of high δ^{56}Fe minerals during clay formation. Notably, Rouxel et al. (2003) found one celadonite vein that had a δ^{56}Fe value of +1.1‰, consistent with the predictions of Polyakov and Mineev (2000). Based on these additional data it seems that the most likely origins of the low δ^{56}Fe values measured in MOR hydrothermal vent fluids are a result of sulfide precipitation as well as basalt-seawater interaction.

The fate of dissolved Fe from MOR vents has been investigated at the Rainbow plume from the mid-Atlantic Ridge. Plume particles were sampled from the buoyant part of the Rainbow plume, proximal to the vent, as well as particles from neutrally buoyant portions of the plume that were more distal from the vent (Severmann et al. 2003). Particles from the buoyant part of the plume have positive δ^{56}Fe values (up to +1.2‰), whereas in the neutrally buoyant sections of the plume, the particles have a near-constant δ^{56}Fe value of −0.2‰ that matches the Fe isotope composition of the vent fluid. The high δ^{56}Fe values of plume particles that were proximal to the vent probably reflect oxidation processes. In the neutrally-buoyant plume, all aqueous Fe(II) had been oxidized and it appears that there was no net loss in Fe because the neutrally buoyant plume particles have the same isotopic composition as the vent fluid. Moreover, metalliferous sediments sampled below the plume match the isotopic composition of the plume particles. The implication of these data is that for at least one plume, the Fe isotope composition of the vent fluid matches that of the plume particles. The Rainbow vent fluid, however, has an unusually high Fe to S ratio and hence it is uncertain if these results can be extrapolated to other plumes that originated from vent fluids that had lower Fe to S ratios.

Iron isotope variations in Fe-Mn nodules

Well-dated layers of an Fe-Mn crust from the Atlantic Ocean provide a potential record of the Fe isotope compositions of this part of the north Atlantic over the past 6 m.y. (Zhu et al. 2000). Layers that span an age from 6 to 1.7 Ma have a constant Fe isotope composition (δ^{56}Fe = −0.69 ± 0.10‰), but layers that are less than 1.7 Ma have increasing δ^{56}Fe values with decreasing age, up to a value of +0.04‰ at 0.15 Ma (Fig. 18). ^{206}Pb/^{204}Pb ratios follow temporal trends that are similar to those of δ^{56}Fe values (Fig. 18). Zhu et al. (2000) concluded that the correlation of Pb and Fe isotope compositions reflect changes in the isotopic composition of lithologic material that was delivered to the north Atlantic Ocean. Based on homogenous Fe isotope composition of clastic sedimentary rocks, modern aerosol particles, and the suspended load of rivers (Beard et al. 2003a) the interpretation of Zhu et al. (2000) cannot be correct. Beard et al (2003a) instead suggested that the origin of the Fe isotope variability for Fe-Mn crusts may be changes in the relative fluxes of Fe from isotopically distinct sources that was delivered to the oceans. Figure 19 shows the fluxes of Fe that are delivered to the modern oceans and the Fe isotope compositions for fluxes that are known. If we assume that Fe

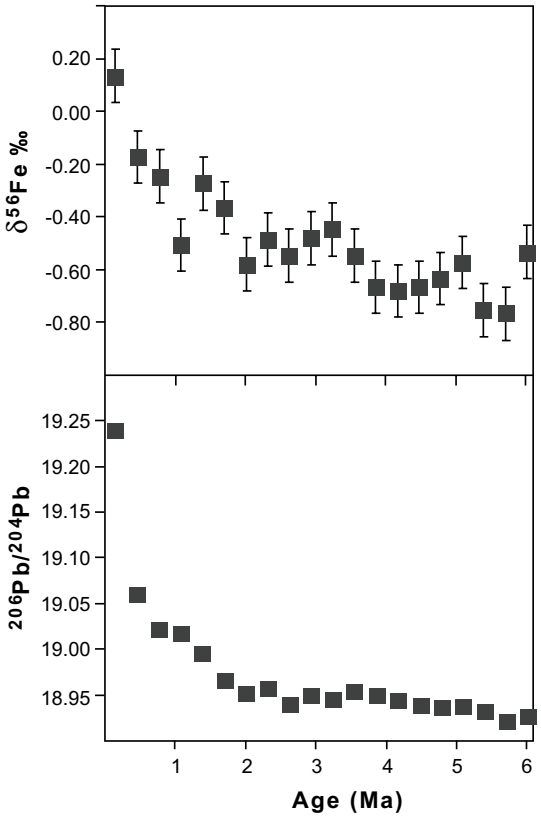

Figure 18. Temporal variations in Fe and Pb isotope composition for layers in Fe-Mn crust BM1969.05 from the Blake Plateau, Atlantic Ocean. Iron isotope data from Zhu et al. (2000) and Pb isotope data and ages from O'Nions et al. (1998) and Reynolds et al. (1999). Modified from Zhu et al. (2000).

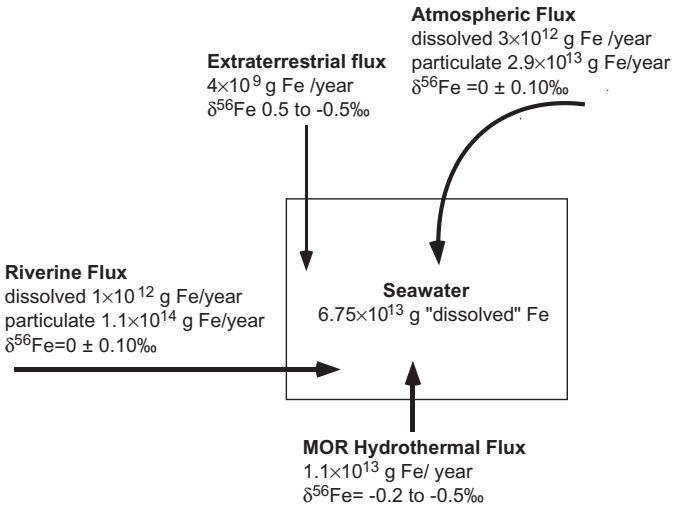

Figure 19. Fluxes of Fe delivered to the oceans and their measured or inferred Fe isotope compositions, modified from Beard et al. (2003a).

delivered to the open oceans results solely from the atmospheric particulate flux and the MOR hydrothermal flux, the δ^{56}Fe values for specific ocean masses may be predicted through simple mixing lines (Fig. 20). Based on this simple model, the calculated Fe isotope composition of the North Atlantic Ocean (δ^{56}Fe = −0.1‰) agrees reasonably well with that measured in the youngest layer of the crust analyzed by Zhu et al. (2000; δ^{56}Fe = +0.13‰). The outer-most layer from a hydrogenous crust from the south-central Pacific Ocean has a δ^{56}Fe value of −0.47‰ (Chu et al. 2003), which also agrees reasonably well with that predicted for the South Pacific Ocean (δ^{56}Fe = −0.32‰; Fig. 20). Superimposed on these global variations are local variations that may reflect differences in the relative contributions of hydrothermal Fe, where Chu et al. (2003) noted distinct temporal trends in δ^{56}Fe values for Fe-Mn crusts from a back-arc basin for localities that were 80 km apart.

This simple two component model for the Fe isotope composition of seawater does not consider the effects of the Fe isotope composition of dissolved Fe from rivers or from rain. Although the dissolved Fe fluxes are small (Fig. 19) the dissolved fluxes may have an important control on the overall Fe isotope composition of the oceans if they represent an Fe source that is preferentially added to the hydrogenous Fe budget that is ultimately sequestered into Fe-Mn nodules. In particular riverine components may be very important in the Pacific Ocean where a significant amount of Fe to the oceans can be delivered from rivers that drain oceanic islands (Sholkovitz et al. 1999). An additional uncertainty lies in how Fe from particulate matter is utilized in seawater. For example, does the solubilization of Fe from aerosol particles result in a significant Fe isotope fractionation, and does Fe speciation lead to Fe isotope fractionation?

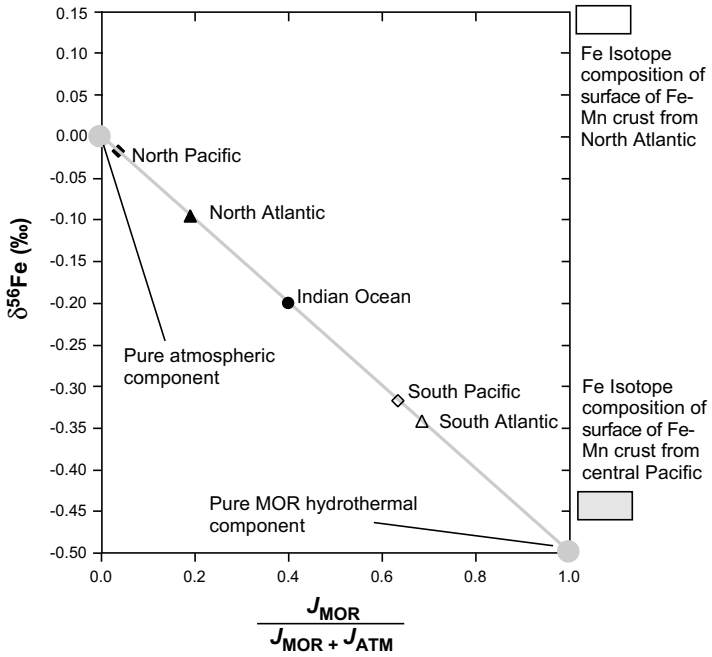

Figure 20. Calculated Fe isotope composition of seawater from different ocean basins based on a simple two-component mixing between Fe from aerosol particles and Fe from mid-oceanic-ridge (MOR) hydrothermal solutions. Atmospheric Fe fluxes (J_{ATM}) for different ocean basins from Duce and Tindale (1991); MOR hydrothermal Fe flux (J_{MOR}) to different ocean basins were proportioned relative to ridge-axis length. Modified from Beard et al. (2003a).

Crucial to unraveling these uncertainties are Fe isotope analyses of the dissolved load from rivers and rainwater, as well as direct analysis of seawater. These analyses will be analytically challenging because of low Fe concentrations. For example, in seawater, it will require 3 to 20 liters of seawater to obtain ~100 ng of Fe which is enough Fe to make a single Fe isotope analysis following the methods of Beard et al. (2003b). In contrast, other methods that rely on using microgram quantities of Fe to achieve large enough Fe ion signals that are not impacted by Ar isobars (e.g., Belshaw et al. 2000) will require significantly more seawater.

One of the key issues for future studies is to determine if the 0.5‰ difference in δ^{56}Fe values between aerosols and hydrothermal fluids is preserved as these materials are dispersed and changed by interaction with seawater. A complete knowledge of the Fe isotope composition of these Fe pools may allow a link to be established between Fe seeding in the open oceans by increased delivery of Fe from aerosols and its possible link to global climate change. For example, Beard et al. (2003a) proposed that the increase in δ^{56}Fe values for the Atlantic Ocean Fe-Mn crust analyzed by Zhu et al. (2000) may have been due to initiation of Northern Hemisphere glaciation at 2.6 Ma, thus increasing detrital loads to the open oceans by ice rafting or by an increase in atmospheric fluxes due to increased mechanical weathering at the expense of chemical weathering. Increases in atmospheric Fe flux delivered to seawater from aerosol particles has been inferred to have occurred during the last glacial maximum (Kumar et al. 1995; Edwards et al. 1998), perhaps indicating that there is a link to glaciation and the content of Fe delivered to the open oceans (Martin 1990). Based on the simple two-component mixing model in Figure 20, such a phenomenon should manifest itself as an increase in δ^{56}Fe values in ocean water as the quantity of atmospheric Fe delivered to the oceans increases. If this model is correct we would expect significant Fe isotope excursions to have occurred in the oceans during the Paleozoic Gondwanaland glaciations (Hambrey and Harland 1981) as well as the large-scale Neoproterozoic glaciations; indeed in the Neoproterozoic (the "snowball Earth" model; Kirschvink 1992), we would expect very large deviations in δ^{56}Fe values for ocean water, possibly shifting to entirely MOR sources.

Banded iron formations

Individual layers in Late Archean to Early Proterozoic BIFs have variable Fe isotope compositions from −2.5 to +1.1‰. Iron isotope variations are correlated with mineralogy, where the δ^{56}Fe values increase in the order: pyrite - Fe carbonates - hematite - magnetite (Johnson et al. 2003a). The δ^{56}Fe values for adjacent magnetite and siderite layers in the Kuruman Iron Formation (South Africa) and the Dales Gorge member of the Brockman Iron Formation (Western Australia) are generally correlated (Fig. 21). The magnetite-siderite fractionations from adjacent layers vary from zero to approximately +1‰, over a 2‰ range in δ^{56}Fe values for siderite. Although it is unknown if magnetite and siderite formed in isotopic equilibrium in many of these samples, it seems unlikely that the relatively large magnetite-siderite fractionations predicted by Polyakov and Mineev (2000) are accurate (Fig. 21). These observations highlight the utility of using natural mineral assemblages to constrain isotopic fractionation factors. Although the magnetite-siderite fractionation factor proposed by Polyakov and Mineev (2000) appears to be correct in sign, it appears to be too large by several per mil at low temperatures. In the case of Fe carbonates, there may be additional complexity due to cation substitution, where ankerite or impure siderite is predicted to have lower δ^{56}Fe values relative to pure siderite (Polyakov and Mineev 2000). Because natural siderites generally contain other cations such as Ca, Mg, and Mn (e.g., Klein and Beukes 1989), the measured $\Delta^{56}Fe_{Magnetite\text{-}Siderite}$ fractionations in Figure 21 are likely to be maximums, and therefore the discrepancy between the measured and predicted fractionations is probably even larger than is illustrated.

Johnson et al. (2003a) presented a preferred set of fluid-mineral fractionation factors based in part on data from BIFs, and proposed that the equilibrium $\Delta^{56}Fe_{Magnetite\text{-}Siderite}$ fractionation is

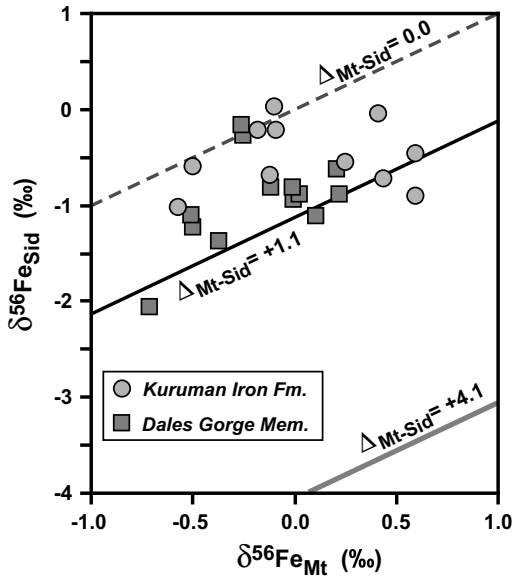

Figure 21. Plot of the measured $\delta^{56}Fe$ value of pairs of magnetite and siderite layers from Banded Iron Formations. Data from Johnson et al. (2003a) and C. Johnson and B. Beard unpublished.

+1.1‰ at 100°C, based on magnetite-siderite pairs where magnetite had positive $\delta^{56}Fe$ values, and many data scatter near this line (Fig. 21). Magnetite that had low $\delta^{56}Fe$ values were thought to have precipitated from unusually low $\delta^{56}Fe$ fluids, and were not considered in deriving the preferred set of fractionation factors. As discussed in the next chapter (Johnson et al. 2004), magnetite that has low $\delta^{56}Fe$ values is now thought to reflect precipitation from aqueous Fe(II) that was produced by bacterial Fe(III) reduction, whereas magnetite that has higher $\delta^{56}Fe$ values seems likely to have precipitated in equilibrium with aqueous Fe(II) that was derived from MOR fluids. These conclusions are possible given the new fluid-mineral fractionation factors that are available (Table 2; Johnson et al. 2004), which did not exist at the time Johnson et al. (2003a) published their study. $\delta^{56}Fe$ values for primary hematite in the Kuruman Iron Formation overlap those of magnetite, and Johnson et al. (2003a) speculated that oxides which have high $\delta^{56}Fe$ values might reflect incomplete oxidation of aqueous Fe(II) by photosynthetic Fe(II) oxidation. It is also possible, however, that abiotic oxidation may produce similar $\delta^{56}Fe$ values (Croal et al. 2004). As highlighted earlier in this chapter, interpretation of the $\delta^{56}Fe$ values of natural ferric oxide/hydroxides likely depends on an understanding of the relative contributions of equilibrium and kinetic effects that may have variable contributions in specific settings.

CONCLUSIONS

The field of Fe isotope geochemistry is rapidly becoming established. Numerous laboratories are making Fe isotope measurements and the emerging picture is that redox processes by both abiologic and biologic means (Johnson et al. 2004) produce some of the most significant Fe isotope variations in nature. The first-order variations in the rock record are now relatively well established by hundreds of analyses of natural samples including many types of low- and high-temperature rocks. Terrestrial igneous rocks and low-C_{org} clastic sedimentary rocks have a narrow range in $\delta^{56}Fe$ values, reflecting the homogenizing process of magmatism and conservative behavior of Fe during weathering under oxygenated surface conditions. Organic-C rich sedimentary rocks and chemically precipitated sediments have

variable $\delta^{56}Fe$ values, reflecting partitioning between minerals and Fe(II)-rich fluids. There are also some significant variations in the Fe isotope composition of extraterrestrial samples where vaporization and condensation of Fe can produce significant Fe isotope variability, particularly in individual chondrules (Kehm et al. 2003), as well as the lunar regolith (Wiesli et al. 2003a). Moreover, there may be important mass-dependent Fe isotope differences between planetary bodies associated with Fe vaporization during planetary accretion (Poitrasson et al. 2002). In some mantle-derived rocks, inter-mineral differences in Fe isotope compositions appear to reflect open-system behavior for olivine, orthopyroxene, and clinopyroxene from spinel peridotites which has lead to significant Fe isotope variability (~0.5‰ in $^{56}Fe/^{54}Fe$). The best case for equilibrium fractionation of Fe isotopes at high temperatures appears to be between garnet and clinopyroxene. Isotopic variability in high-temperature environments, however, appears to be rarely expressed in crustal rocks apparently reflecting homogenization during magma generation, as recorded in the constant Fe isotope composition of a wide variety of igneous rocks ($\delta^{56}Fe = 0.00 \pm 0.05$‰, 1σ; Beard et al. 2003b), as well as most low-C_{org} clastic sedimentary rocks.

The ability to understand measured Fe isotope variations in nature, however, is limited because the database of well constrained Fe isotope fractionation factors is small. Determination of equilibrium fractionation factors provides the broadest application to different environments, although kinetic effects are also important, particularly in cases where reactions in nature may be rapid, such as oxidation of aqueous Fe(II). It is critical that experimental investigations take a mechanistic approach to determining isotopic fractionation, given the fact that fluid-mineral fractionations at low temperature must rely on synthesis methods. Additionally, as a check on these laboratory investigations, it is important to conduct studies on modern natural samples where the Fe isotope compositions of the fluids and minerals may be determined. The analysis of fluids that have low Fe contents, but overall high ionic strengths (such as pore fluids or seawater) will be analytically challenging, requiring superb chemical purification techniques and mass spectrometry methods that only require nanogram quantities of Fe for a mass analysis.

ACKNOWLEDGMENTS

We thank Ashley Hubbard, Rebecca Poulson, Silke Severman, Joe Skulan, Sue Welch, René Wiesli, and Kosei Yamaguchi for their assistance in the lab and numerous helpful discussions. We thank three anonymous reviewers and Francis Albarède for their helpful comments. We acknowledge support from NSF and NASA for our Fe isotope research.

REFERENCES

Albarède F, Beard BL (2004) Analytical methods for non-traditional isotopes. Rev Mineral Geochem 55: 113-151

Alexander CMO'D, Wang J (2001) Iron isotope in chondrules: implications for the role of evaporation during chondrule formation. Meteoritics Planet Sci 36:419-428

Anbar AD (2004) Iron stable isotopes: beyond biosignatures. Earth Planet Sci Lett 217:223-236

Anbar AD, Roe JE, Barling J, Nealson KH (2000) Nonbiological fractionation of iron isotopes. Science 288: 126-128

Anbar AD, Jarzecki AA, Spiro TG (2004) Theoretical investigation of iron isotope fractionation between $Fe(H_2O)_6^{3+}$ and $Fe(H_2O)_6^{2+}$: implications for iron stable isotope geochemistry. Geochim Cosmochim Acta, in press

Archer C, Vance DA (2002) Large fractionations in Fe, Cu, and Zn isotopes associated with Archean microbially mediated sulphides. Geochim Cosmochim Acta 66:A26

Arthur MA, Anderson TF, Kaplan IR (1983) Stable isotopes in sedimentary geology. SEPM short course, 10, 432 pp

Beard BL, Johnson CM (1999) High Precision iron isotope measurements of terrestrial and lunar material. Geochim Cosmochim Acta 63:1653-1660

Beard BL, Johnson CM (2004) Inter-mineral Fe isotope variations in mantle derived rocks and implications for the Fe geochemical cycle. Geochim Cosmochim Acta, in press

Beard BL, Johnson CM, Cox L, Sun H, Nealson KH, Aguiliar C (1999) Iron isotope biosignatures. Science 285:1889-1892

Beard BL, Johnson CM, Von Damm KL, Poulson RL (2003a) Iron isotope constraints on Fe cycling and mass balance in the oxygenated Earth oceans. Geology 31:629-632

Beard BL, Johnson CM, Skulan JL, Nealson KH, Cox L, Sun H. (2003b) Application of Fe isotopes to tracing the geochemical and biological cycling of Fe. Chem Geol 195:87-117

Belshaw NS, Zhu XK, Guo Y, O'Nions RK (2000) High precision measurement of iron isotopes by plasma source mass spectrometry. Int J Mass Spectrom 197:191-195

Berger A, von Blanckenburg F (2001) High-temperature fractionation of Fe isotopes. Eos Trans. Am Geophys Union 82:V21A-0958

Bergquist B, Boyle E (2002) Iron isotopic composition of Amazon River. EOS Trans. Am Geophys Union 83: OS12C-0290

Bernatowicz TJ, Nichols RH, Hohenberg CM (1994) Origin of amorphous rims on lunar soil grains. Lunar Planet Sci Conf XXV, 105-106

Beukes NJ, Klein C (1992) Models for Iron-formation deposition. In: The Proterozoic Biosphere: A multidisciplinary study. Schopf JW, Klein C (eds) Cambridge University Press, New York, p 147-151

Birck JL (2004) An overview of isotopic anomalies in extraterrestrial materials and their nucleosynthetic heritage. Rev Mineral Geochem 55:25-64

Brantley SL, Liermann L, Bullen TD (2001) Fractionation of Fe isotopes by soil microbes and organic acids. Geology 29: 535-538

Bruland KW, Odonat JR, Hutchins DA (1991) Interactive influences of bioactive trace metals on biological production in oceanic waters. Limnol Oceanography 36:1555-1577

Bullen TD, White AF, Childs CW, Vivet DV, Schultz MS (2001) Demonstration of significant abiotic iron isotope fractionation in nature. Geology 29:699-702

Bullen TD, White AF, Childs CW (2003) Comment on "Isotopic fractionation between Fe(III) and Fe(II) in aqueous solutions" by Clark Johnson et al., [Earth Planet Sci Lett 195 (2002) 141-153]. Earth Planet Sci Lett 206:229-232

Butler IP, Archer C, Rickard D, Vance D, Oldroyd A (2003) Fe isotope fractionation during Fe(II) monosulfide precipitation from aqueous Fe solutions at pH 8 and ambient temperature. Geochim Cosmochim Acta 67:A51

Canfield DE (1997) The geochemistry of river particulates from the continental USA: major elements. Geochim Cosmochim Acta 61:3349-3365

Chu N-C, Johnson CM, Beard BL, German CR, Nesbitt RW, Usui A (2003) Secular Fe isotope variations in the central Pacific Ocean. Geochim Cosmochim Acta 67:A66

Clayton DD (1999) Radiogenic iron. Meteor Planet Sci 34:A145-A160

Clayton RN (1993) Oxygen isotopes in meteorites. Ann Rev Earth Planet Sci 21:115-149

Clayton RN, Mayeda TK, Hurd JM (1974) Loss of oxygen, silicon, sulfur, and potassium from the lunar regolith. Proc Lunar Sci Conf 5:1801-1809

Criss RE (1999) Principles of stable isotope distribution. Oxford Univ Press, New York

Croal LR, Johnson CM, Beard BL, Newman DK (2004) Iron isotope fractionation by anoxygenic Fe(II)-phototrophic bacteria. Geochim Cosmochim Acta: in press

Duce RA, Tindale NW (1991) Atmospheric transport of iron and its deposition in the ocean. Limnol Oceanography 36:1715-1726

Edwards R, Sedwick PN, Morgan V, Boutron CF, Hong S (1998) Iron in ice cores from Law Dome, east Antarctica: implications for past deposition of aerosol iron. Ann Glaciol 27:365-370

Eiler JM (2001) Oxygen isotope variations of basaltic lavas and upper mantle rocks. Rev Mineral Geochem 43:319-364

Epstein S, Taylor HP (1971) O^{18}/O^{16}, Si^{30}/Si^{28}, D/H, and C^{13}/C^{12} ratios in lunar samples. Proc Lunar Sci Conf 2:1421-1441

Esat TM, Taylor SR (1992) Magnesium isotope fractionation in lunar soils. Geochim Cosmochim Acta 56: 1025-1031

Ewers WE (1983) Chemical factors in the deposition and diagenesis of banded iron-formation. In: Iron Formations: Facts and Problems. Trendall AF, Morris RC (eds) Elsevier, Amsterdam, p 491-512

Fantle MS, DePaolo DJ (2002) The isotopic composition of continental iron and implications for the global Fe cycle. EOS Trans Am Geophys Union 83:V22B-1234

Grandstaff DE (1980) Origin of uraniferous conglomerates at Elliot Lake, Canada and Witwatersrand, South Africa, implications for oxygen in the Precambrian atmosphere. Precambrian Research 13:1-26
Gregory RT, Criss RE (1986) Isotopic exchange in open and closed systems. Rev Mineral 16:91-128
Hambrey MJ, Harland WB (1981) Earth's Pre-Pleistocene Glacial Record, Cambridge Univ Press, Cambridge
Hapke B (2001) Space weathering from Mercury to the asteroid belt. J Geophys Res 106:10039-10073
Hapke B, Cassidy W, Wells E (1994) Vapor deposits in the lunar regolith: Technical comment. Science 264: 1779
Herzog GF, Xue S, Hall GS, Nyquist LE, Shih C-Y, Wiesmann H, Brownlee DE (1999) Isotopic and elemental composition of iron, nickel, and chromium, in type I deep-sea spherules: Implications for origin and composition of the parent micrometeoroids. Geochim Cosmochim Acta 63:1443-1457
Holland HD (1994) Early Proterozoic atmospheric change. In: Early Life on Earth, Noble Symposium No 84. Bengston S (ed), Columbia University Press, p. 237-244
Humayun M, Clayton RN (1995) Precise determination of the isotopic composition of potassium: application to terrestrial rocks and lunar soils. Geochim Cosmochim Acta 59:2115-3130
Johnson CM, Beard BL (1999) Correction of instrumentally produced mass fractionation during isotopic analysis of Fe by thermal ionization mass spectrometry. Int J Mass Spectrom 193:87-99
Johnson CM, Skulan JL, Beard BL, Sun H, Nealson KH, Braterman PS (2002) Isotopic fractionation between Fe(III) and Fe(II) in aqueous solutions. Earth Planet Sci Lett 195:141-153
Johnson CM, Beard BL, Beukes NJ, Klein C, O'Leary JM (2003a) Ancient geochemical cycling in the Earth as inferred from Fe isotope studies of banded iron formations from the Transvaal Craton. Contrib Mineral Petrol 144:523-547
Johnson CM, Beard BL, Braterman PS, Welch SA (2003b) Reply to comment on 'Isotopic fractionation between Fe(III) and Fe(II) in aqueous solutions' by Thomas D. Bullen, Arthur F. White and Cyril W. Childs. Earth Planet Sci Lett 206:233-236
Johnson TM, Bullen TD (2004) Mass-dependent fractionation of selenium and chromim isotopes in low-temperature environments. Rev Mineral Geochem 55:289-317
Johnson KS, Gordon RM, Coale KH (1997) What controls dissolved iron concentrations in the world ocean? Mar Chem 57:137-161
Kasting JF, Liu SC, Honahue TM (1979) Oxygen levels in the prebiological atmosphere. J Geophys Res 84: 3097-3107
Kehm K, Hauri EH, Alexander CMO'D, Carlson RW (2003) High precision iron isotope measurements of meteoritic material by cold plasma ICP-MS. Geochim Cosmochim Acta 67:2879-2891
Keller LP, McKay DS (1993) Discovery of vapor deposits in the lunar regolith. Science 261:1305-1307
Kirschvink JL (1992) Late Proterozoic low-latitude global glaciation: the snowball Earth. In: The Proterozoic Biosphere: A multidisciplinary study. Schopf JW, Klein C (eds) Cambridge University Press, New York, p 147-151
Klein C, Beukes NJ (1989) Geochemistry and sedimentology of a facies transition from limestone to iron-formation deposition in the early Proterozoic Transvaal Supergroup, South Africa. Econ Geol 84:1733-1774
Kumar N, Anderson RF, Mortlock RA, Froelich PN, Kubik P, Dittrich-Hannen B, Suter M (1995) Increased biological productivity and export production in the glacial southern ocean. Nature 378:675-680
Malinovsky D, Stenberg A, Rodushkin I, Andren H, Ingri J, Öhlander B, Baxter DC (2003) Performance of high resolution MC-ICP-MS for Fe isotope ratio measurements in sedimentary geologic materials. J Anal At Spectrom 18:687-695
Mandernack KW, Bazylinski DA, Shanks WC, III, Bullen TD (1999) Oxygen and iron isotope studies of magnetite produced by magnetotactic bacteria. Science 285:1892-1896
Martin JH (1990) Glacial-interglacial CO_2 change: the iron hypothesis. Paleooceanography 5:1-13
Martin JH (1992) Iron as a limiting factor in oceanic productivity. In: Primary productivity and biogeochemical cycles in the sea. Falkowski P, Woodhead AD (eds) Plenum, New York, p 123-127
Martin JH, Fitzwater EE (1988) Iron limits phytoplankton growth in the northeast Pacific subarctic. Nature 331:341-343
Martin JH, Gordon RM (1988) Northeast Pacific iron distributions in relation to phytoplankton productivity. Deep-Sea Res 34:267-285
Martin JH, Gordon RM, Fitzwater S, Broenkow WW (1989) VERTEX: Phytoplankton/iron studies in the Gulf of Alaska. Deep-Sea Res 36:649-680
Martin JH, Coale KH, Johnson KS, et al. (1994) Testing the iron hypothesis in ecosystems of the Equatorial Pacific Ocean. Nature 371:123-129
Matthews A, Zhu X-K, O'Nions RK (2001) Kinetic iron stable isotope fractionation between iron (-II) and (-III) complexes in solution. Earth Planet Sci Lett 192:81-92

Matthews A, Morgans-Bell HS, Emmanuel S, Jenkyns HC, Erel Y, Halicz L (2004) Controls on iron-isotope fractionation in organic-rich sediments. Geochim Cosmochim Acta, in press

Millero FJ, Yao W, Aicher J (1995) The speciation of Fe(II) and Fe(III) in natural waters. Marine Chemistry 50:21-39

Morris RV (1976) Surface exposure indices of lunar soils: a comparative FMR study. Proc Lunar Planet Sci Conf 7:315-335

Mullane E, Russel SS, Gounelle M (2002) Iron isotope fractionation within a differentiated asteroidial sample suite. 65th Annual Meteoritical Society Meeting, abstract number 5157

Mullane E, Russel SS, Gounelle M, Mason TFD (2003a) Iron isotope composition of Allende and Chainpur chondrules: effects of equilibration and thermal history. Lunar Planet Sci Conf XXXIV, abstract number 1027

Mullane E, Russell SS, Gounelle M, Mason TFD (2003b) Iron isotope composition of Allende matrix, CAIs and chondrules. 66th Annual Meteoritical Society Meeting, abstract number 5117

Mullane E, Russell SS, Gounelle M, Mason TFD, Weiss D, Coles B (2003c) Magmatic and impact processing on the HED parent body: Effects on iron isotope signatures. Geochim Cosmochim Acta 67:A311

O'Nions RK, Frank M, von Blanckenburg F, Ling H-F (1998) Secular variation of Nd and Pb isotopes in ferromanganese crusts from the Atlantic, Indian, and Pacific Oceans. Earth Planet Sci Lett 155:15-28

Poitrasson F, Halliday AN, Lee D, Levasseur S, Teutsch N (2002) Origin of the Moon unveiled by its heavy iron isotope composition. Eos Trans Am Geophys Union 83:P11A-0355

Polyakov VB, Mineev SD (2000) The use of Mössbauer spectroscopy in stable isotope geochemistry. Geochim Cosmochim Acta 64:849-865

Poulson RL, Beard BL, Johnson CM (2003) Investigating isotopic exchange between dissolved aqueous and precipitated iron species in natural and synthetic systems. Geochim Cosmochim Acta 67:A382

Reynolds BC, Frank M, O'Nions RK (1999) Nd- and Pb-isotope time series from Atlantic ferromanganese crusts: implications for changes in provenance and paleocirculation over the last 8 Myr. Earth Planet Sci Lett 173:381-396

Roe JE, Anbar AD, Barling J (2003) Nonbiological fractionation of Fe isotopes: evidence of an equilibrium isotope effect. Chem Geol 195:69-85

Rouxel O, Dobbek N, Ludden J, Fouquet Y (2003) Iron isotope fractionation during oceanic crust alteration. Chem Geol 202:155-182

Rouxel O, Fouquet Y, Ludden JN (2004) Subsurface processes at the Lucky Strike Hydrothermal Field, Mid-Atlantic Ridge: Evidence from sulfur, selenium, and iron isotopes. Geochim Cosmochim Acta, submitted

Russell WA, Papanastassiou DA, Tombrello TA, Epstein S (1977) Ca isotope fractionation on the moon, Proc Lunar Sci Conf 8:3791-3805

Sands DG, Rosman KJR, Laeter de JR (2001) A preliminary study of cadmium mass fractionation in lunar soils. Earth Planet Sci Lett 186:103-111

Schauble EA (2004) Applying stable isotope fractionation theory to new systems. Rev Mineral Geochem 55: 65-111

Schauble EA, Rossman GR, Taylor HP (2001) Theoretical estimates of equilibrium Fe-isotope fractionations from vibrational spectroscopy. Geochim Cosmochim Acta 65:2487-2497

Severmann S, Larsen O, Palmer MR, Nüster J (2002) The isotopic signature of Fe-mineralization during early diagenesis. Geochim Cosmochim Acta 66:A698

Severmann S, German CR, Edmonds HN, Beard BL, Johnson CM (2003) The modification of hydrothermal Fe-isotopic signature during plume-processing. Geochim Cosmochim Acta 67:A424

Sharma M, Polizzotto M, Anbar AD (2001) Iron isotopes in hot springs along the Juan de Fuca Ridge. Earth Planet Sci Lett 194:39-51

Sholkovitz ER, Elderfield H, Szymczak R, Casey K (1999) Island weathering: riverine sources of rare earth elements to the western Pacific Ocean. Marine Chem 68:39-57

Skulan JL, Beard BL, Johnson CM (2002) Kinetic and equilibrium Fe isotope fractionation between aqueous Fe(III) and hematite. Geochim Cosmochim Acta 66:2995-3015

Sumner DY (1997) Carbonate precipitation and oxygen stratification in Late Archean seawater as deduced from facies and stratigraphy of the Gamohaan and Frisco Formations, Transvaal Supergroup, South Africa. Am J Sci 297:455-487

Taylor LA, Pieters CM, Keller LP, Morris RV, McKay DS (2001) Lunar Mare Soils: Space weathering and the major effect of surface-correlated nanophase Fe. J Geophys Res 106:27985-27999

Taylor PDP, Maeck R, De Bièvre P (1992) Determination of the absolute isotopic composition and Atomic Weight of a reference sample of natural iron. Int J Mass Spectrom Ion Proc 121:111-125

Taylor PDP, Maeck R, Hendricks F, De Bièvre P (1993) The gravimetric preparation of synthetic mixtures of iron isotopes. Int J Mass Spectrom Ion Proc 128:91-97

Thode HG, Rees CE (1976) Sulphur isotopes in grain size fractions of lunar soils, Proc Lunar Sci Conf 7: 459-468

Völkening J, Papanastassiou DA (1989) Iron isotope anomalies. Astrophys J 347:L43-L46

Walczyk T, von Blanckenburg F (2002) Natural iron isotope variations in human blood. Science 295:2065-2066

Wasson JT, Choi B-G (2003) Main-group pallasites: Chemical composition, relationship to IIIAB irons, and origin. Geochim Cosmochim Acta 67:3079-3096

Welch SA, Beard BL, Johnson CM, Braterman PS (2003) Kinetic and equilibrium Fe isotope fractionation between aqueous Fe(II) and Fe(III). Geochim Cosmochim Acta 67:4231-4250

Weyer S, Schwieters JB (2003)High precision Fe isotope measurements with high mass resolution MC-ICPMS. Int J Mass Spectrom 226:355-368

Wiesli RA, Beard BL, Taylor LA, Johnson CM (2003a) Space weathering processes on airless bodies: Fe isotope fractionation in the lunar regolith. Earth Planet Sci Lett 216:457-465

Wiesli RA, Beard BL, Johnson CM (2003b) Experimental determination of Fe isotope fractionation between aq. Fe(II), "green rust", and siderite. Geochim Cosmochim Acta 67:A533

Williams H, Lee D-C, Levasseur S, Teutsch N, Poitrasson F., Halliday AN (2002) Iron isotope composition of mid-ocean ridge basalts and mantle peridotites. Geochim Cosmochim Acta 66:A838

Yamaguchi KE, Beard BL, Johnson CM, Ohkouchi N, Ohmoto H (2003) Iron isotope evidence for redox stratification of the Archean oceans. Geochim Cosmochim Acta 67:550

Zhu XK, O'Nions RK, Guo Y, Reynolds BC (2000) Secular variation of iron isotopes in north Atlantic Deep Water. Science 287:2000-2002

Zhu XK, Guo Y, O'Nions RK, Young ED, Ash RD (2001) Isotopic homogeneity of iron in the early solar nebula. Nature 412:311-313

Zhu XK, Guo Y, Williams RJP, O'Nions RK, Matthews A, Belshaw NS, Canters GW, de Waal EC, Weser U, Burgess BK, Salvato B (2002) Mass fractionation processes of transition metal isotopes. Earth Planet Sci Lett 200:47-62